

Semiparametric bivariate extreme-value copulas

Javier Fernández Serrano

javierfdez_90@hotmail.com

Abstract

Extreme-value copulas arise as the limiting dependence structure of component-wise maxima. Defined in terms of a functional parameter, they are one of the most widespread copula families due to its flexibility and ability to capture asymmetry. Despite this, meeting the complex analytical properties of this parameter in an unconstrained setting still remains a challenge, restricting most uses to either models with very few parameters or non-parametric models. On this paper we focus on the bivariate case and propose a novel approach for estimating this functional parameter in a semiparametric manner. Our procedure relies on a series of basic transformations starting from a zero-integral spline. Spline coordinates are fit through maximum likelihood estimation, leveraging gradient optimization, without imposing further constraints. We conduct several experiments on both simulated and real data. Specifically, we test our method on scarce data gathered by the gravitational wave detection LIGO and Virgo collaborations.

Keywords— extreme-value copula, bivariate copula, semiparametric models, Pickands dependence function, Williamson’s transform, Bayes space, zero-integral splines, Python, automatic differentiation, Gini coefficient

1 Introduction

Copulas allow to model multivariate dependencies independently from the distribution of the corresponding margins. In the bivariate case, *Sklar’s* theorem [42] states that any joint probability cumulative distribution function (CDF) H can be decomposed as

$$H(x, y) = C(F(x), G(y)), \quad (1)$$

where F and G are the first and second margin CDFs from H and C is the so-called copula function. The latter is defined over $[0, 1]^2$ and has the analytical properties of a restricted bivariate joint CDF with uniform margins on $[0, 1]$. Uniqueness of C is ensured provided that F and G are continuous; otherwise, it is uniquely determined on $\text{Ran}(F) \times \text{Ran}(G)$. Conversely, given univariate CDFs F and G and a copula C , the H in (1) is a joint CDF with margins F and G .

The unique part of a copula from a joint CDF H can be retrieved by means of the *quasi-inverses* [42] $F^{[-1]}$ and $G^{[-1]}$ of F and G , respectively:

$$C(u, v) = H(F^{[-1]}(u), G^{[-1]}(v)). \quad (2)$$

Many important stochastic dependency properties solely depend on the copula *linking* the margins [42, 7]. Among these, we encounter concordance measures as Kendall's tau or Spearman's rho, tail dependence coefficients and even mutual information, which is equivalent to copula entropy [36].

The procedure (2) allows to build *implicit* copulas from known bivariate joint CDFs, for instance, the Gaussian copula or the Student's copula [7]. Other copulas can be *explicitly* constructed in closed form, most notably Archimedean [41], extreme-value [28] or archimax copulas [10]. Either of these copula *meta-families* is defined in terms of one or more functional parameters. Particular instantiations of such functions give rise to parametric copula families like Clayton's or Frank's (Archimedean), Tawn's (extreme-value) or Gumbel's (both Archimedean and extreme-value).

On this paper we will focus on extreme-value copulas (EVC), which arise as the limiting dependence structure of component-wise maxima [28].

1.1 Extreme-value copulas

Consider a sequence $\{(X_{1,i}, X_{2,i})\}_{i=1}^{\infty}$ of independent and identically distributed random 2-vectors with copula C and continuous margins. Then, build the sequence of partial maxima

$$\{(M_{1,n}, M_{2,n})\}_{n=1}^{\infty}, \text{ where } M_{j,n} = \max_{i \leq n} \{X_{j,i}\}. \quad (3)$$

The copula of the n -th element in the sequence (3) is given by

$$(u, v) \mapsto C(u^{1/n}, v^{1/n})^n. \quad (4)$$

A copula C is said to be an EVC if it is the weak limit of the sequence (4), i.e.,

$$\lim_{n \rightarrow \infty} C^*(u^{1/n}, v^{1/n})^n = C(u, v), \quad (5)$$

for all $(u, v) \in [0, 1]^2$ and some underlying copula C^* . Interestingly, it turns out that C is an EVC if and only if it can be expressed as

$$C(u, v) = \exp \left\{ \log(uv) A \left[\frac{\log(u)}{\log(uv)} \right] \right\}, \text{ for } u, v \in (0, 1)^2, \quad (6)$$

where $A : [0, 1] \rightarrow \mathbb{R}$, known as the Pickands function, satisfies the following two constraints:

1. $\max\{t, 1-t\} \leq A(t) \leq 1$, for all $t \in [0, 1]$.
2. A is convex.

The first constraint confines the graph of A to a triangular subset of $[0, 1]^2$ and effectively makes $\text{Ran}(A) \subset [1/2, 1]$. It can also be replaced with an equivalent constraint [29] concerning the behaviour of A at the endpoints, namely $A(0) = A(1) = 1$, $A'(0^+) \geq -1$ and $A'(1^-) \leq 1$. The lines $\{(t, 1-t) : t \in [0, 1]\}$ and $\{(t, t) : t \in [0, 1]\}$ are called the *support* lines of the Pickands function. All these elements are depicted in Figure 1. On the other hand, the convexity constraint can be replaced by $A''(t) \geq 0$ for all $t \in [0, 1]$ whenever A is twice differentiable [29], as will be the case all along this paper.

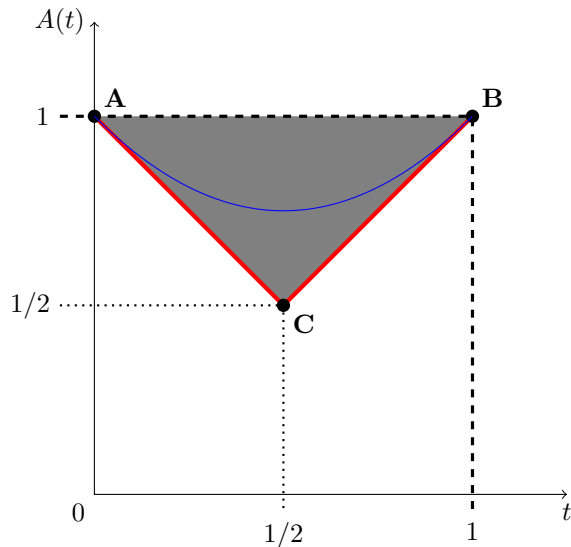


Figure 1: Pickands function geometry. The admissible region for its graph is colored in gray. Support lines are colored in red. Points **A**, **B** and **C** will be referenced later on when describing our method. An example of Pickands function, namely $A(t) = t^2 - t + 1$, is drawn in blue.

The lower bound $\max\{t, 1-t\}$ yields $C(u, v) = \min\{u, v\}$, the perfect dependence copula, whereas the upper bound, $A \equiv 1$, corresponds to the independence copula $C(u, v) = uv$.

It is easy to check that any convex combination of Pickands functions results in a Pickands function. Also, given a Pickands function A , the change of variable $\bar{A} : t \mapsto A(1-t)$ yields a Pickands function too. In fact, it can be shown that the symmetry of C in (6), in the sense that $C(u, v) = C(v, u)$, is equivalent to the symmetry of A with respect to the $\{t = 1/2\}$ axis [19], i.e., $A(t) = \bar{A}(t)$ for all $t \in [0, 1]$. For this reason, some authors [19] define EVC equivalently by taking $\log(v)/\log(uv)$ as the argument of A in (6). Symmetry in the context of copulas is known as *exchangeability*. Taking both properties into consideration, it follows that $\hat{A} : t \mapsto (A(t) + \bar{A}(t))/2$ is a symmetrical Pickands function and, hence, the subsequent copula will be exchangeable.

The partial derivatives of an EVC C relate to A according to the equations [19, 15]

$$\begin{aligned} \frac{\partial C}{\partial u}(u, v) &= \frac{C(u, v)}{u} [A(t) + (1-t)A'(t)] \\ \frac{\partial C}{\partial v}(u, v) &= \frac{C(u, v)}{v} [A(t) - tA'(t)] \end{aligned}, \quad (7)$$

where $t = \log(u)/\log(uv)$.

For EVCs, correlation coefficients like Kendall's tau and Spearman's rho can be computed as integrals involving A [33]. Even simpler, Blomqvist's beta [45] and the upper tail index can be expressed in terms of $A(1/2)$ as, respectively,

Family	$A_\theta(t)$	θ range
Gumbel	$[t^\theta + (1-t)^\theta]^{1/\theta}$	$[1, \infty)$
Galambos	$1 - [t^{-\theta} + (1-t)^{-\theta}]^{-1/\theta}$	$(0, \infty)$
Hüssler-Reiss	$\varphi(t) + \varphi(1-t), \varphi(t) \equiv t \Phi\left(\theta + \frac{1}{2\theta} \log\left(\frac{t}{1-t}\right)\right)$	$(0, \infty)$

Table 1: Main one-parameter EVC families [33]. The Φ in the Hüssler-Reiss designates the standard normal CDF. The above families are all symmetrical. Asymmetry can be induced by Khoudraji's procedure.

$$\beta = 4^{1-A(1/2)} - 1, \quad (8) \quad \lambda = 2(1 - A(1/2)). \quad (9)$$

From (8) and (9) we see that both measures are related through $\beta = 2^\lambda - 1$ and that $\beta = \lambda = 1$ is attained if and only if $A(1/2) = 1/2$, which is equivalent to A producing the perfect dependence copula. Except for the case of perfect dependence, EVCs do not exhibit lower tail dependence.

Example 1. The function $A(t) = t^2 - t + 1$ in Figure 1 is a Pickands function since $A(0) = A(1) = 1$, $A'(0) = -1$, $A'(1) = 1$ and $A''(t) = 2$ for all $t \in (0, 1)$. Additionally, $A(t) = A(1-t)$, thus the subsequent EVC is exchangeable. It can also be checked that it is the lowest degree polynomial Pickands function such that $A(1/2) = 3/4$, thus producing $\beta = \lambda = 1/2$.

The Pickands function can yet be expressed [29] as

$$A(t) = \int_0^1 \max\{t(1-z), z(1-t)\} d\mathcal{H}(z), \quad (10)$$

where \mathcal{H} is the so-called *spectral* measure on $[0, 1]$: a finite measure satisfying $\int_0^1 z d\mathcal{H}(z) = 1$. Furthermore, under absolute continuity of A' [29], \mathcal{H} admits a decomposition

$$\mathcal{H}(B) = \mathcal{H}_0 \mathbf{1}_B(0) + \int_B \eta(z) dz + \mathcal{H}_1 \mathbf{1}_B(1), \quad (11)$$

where $\mathbf{1}_B$ denotes the indicator function on B , $\eta = A''$ almost everywhere on $(0, 1)$ and

$$\mathcal{H}_x \equiv \mathcal{H}(\{x\}) = \begin{cases} 1 + A'(0^+), & \text{if } x = 0 \\ 1 - A'(1^-), & \text{if } x = 1 \end{cases}, \quad (12)$$

satisfy $0 \leq \mathcal{H}_x \leq 1$, $x = 0, 1$.

Neither the original constraints of A (support and convexity) nor the spectral measure ones of \mathcal{H} (non-negativity and unitary first moment) can be easily attained through conventional approximation methods: polynomials, splines, etc. Instead, the use of EVCs has been primarily centered on a few symmetrical one-parameter families, some of which are collected in Table 1.

The following procedure by Khoudraji [34] and described in [19] allows to obtain symmetrical copulas from asymmetrical ones. Given a copula C (not necessarily symmetrical [44]) and $\alpha, \beta \in (0, 1]$, the following will also be a copula:

$$C_{\alpha, \beta}(u, v) = u^{1-\alpha} v^{1-\beta} C(u^\alpha, v^\beta). \quad (13)$$

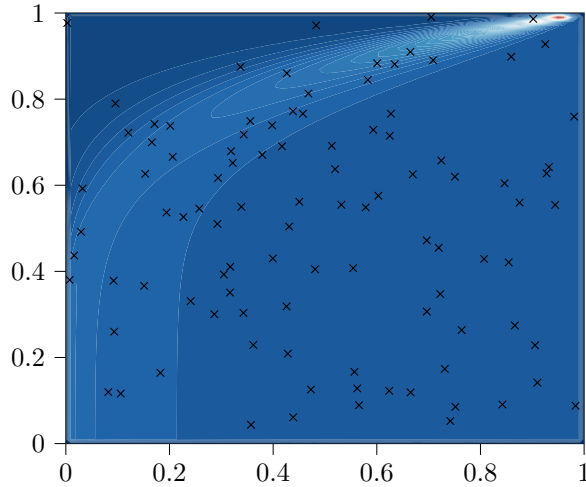


Figure 2: Sample-density plot of an instance of the Tawn family (Gumbel family with asymmetry induced by Khoudraji's procedure) with parameters $\theta = 5.0$, $\alpha = 0.5$ and $\beta = 0.1$.

Moreover, if C in (13) is an EVC, the corresponding $C_{\alpha,\beta}(u, v)$ will also be EVC, with Pickands function given by

$$A_{\alpha,\beta}(t) = (1-t)(1-\alpha) + t(1-\beta) + [(1-t)\alpha + t\beta]A \left[\frac{t\beta}{(1-t)\alpha + t\beta} \right]. \quad (14)$$

In general, if C is symmetrical, $C_{\alpha,\beta}$ will be asymmetrical whenever $\alpha \neq \beta$. The asymmetrical extensions by means of (14) of the Gumbel and Galambos families in Table 1 are known as the Tawn and Joe copula families, respectively [19]. Figure 2 shows an example of the former.

On this paper we propose a novel approach for constructing a Pickands function that can be flexibly fit to data. Our method yields a highly-parameterized approximation, barely relying on a few relatively weak assumptions, that meets all the constraints for a Pickands function while remaining computationally tractable.

1.2 Organization

The rest of the paper is organized as follows. In section 2 we will provide a review on previous EVC modelling approaches. Next, section 3 is fully devoted to our own method, where we address both theoretical and practical issues. Our method will later be tested on a simulation study in section 4 and also on real data in section 5. Finally, in section 6 we provide further comments on the performance and general possibilities of our method and eventually propose some future lines of work in section 7.

2 Related work

Vettori, Huser, and Genton provide a comprehensive literature review on EVC, comparing different methods and focusing on key aspects, such as constraint compliance and applicability to higher dimensions [52]. They find that the most relevant methods fall into one of two categories, namely non-parametric or parametric estimation. In general, non-parametric models demonstrate greater flexibility than parametric ones, especially when dealing with asymmetrical data, at the expense of higher variance. In dimensions higher than 2 and with mild asymmetry, parametric models, using Khoudraji's asymmetric extension, perform well against non-parametric ones.

One of the first estimators for the Pickands function was proposed by Pickands himself in [43] in the context of joint bivariate survival analysis [32]. Given a random sample $\{(X_i, Y_i)\}_{i=1}^n$ from a bivariate extreme-value distribution, he proposes the following estimator:

$$\hat{A}_n(t) = \left\{ \frac{1}{n} \sum_{i=1}^n \min[(1-t)^{-1}X_i, t^{-1}Y_i] \right\}^{-1}. \quad (15)$$

In general, (15) is almost surely non-convex over $[0, 1]$ [32]. Several authors have proposed corrections for (15) to be convex. Pickands himself proposed in [43] to use the greatest convex minorant of \hat{A}_n , which still remains one of the most practical and efficient approaches of its kind.

Perhaps the most widespread non-parametric method is due to Capéreaù, Fougères, and Genest [8], from which it borrows its name CFG. They observe that given a random sample $\{(U_i, V_i)\}_{i=1}^n$ from an EVC with Pickands function A , the transformation $Z_i = \log U_i / \log(U_i V_i)$ is distributed according to

$$H(z) = z + z(1-z) \frac{A'(z)}{A(z)}. \quad (16)$$

From here, one can empirically estimate H with some \tilde{H} and solve (16) for an estimator

$$\tilde{A}(t) = \exp \left\{ \int_0^t \frac{\tilde{H}(z) - z}{z(1-z)} dz \right\}. \quad (17)$$

Although the estimator \tilde{A} can be directly used, it will not be convex in general. Jiménez, Villa-Diharce, and Flores propose two modified versions of the CFG estimator that do satisfy the convexity constraint [32].

According to [52], most estimation methods until the early 2010's are variants of either Pickands's, CFG or both. More recent advances have focused on several uses of polynomials and splines. For instance, Guillotte and Perron study the conditions under which a polynomial, expressed in Bernstein form, is a Pickands function. Marcon et al. use Bernstein-Bézier polynomials to enforce some Pickands function constraints [39]. Cormier, Genest, and Nešlehová use constrained quadratic smoothing B-splines to develop a compliant Pickands estimator in a non-parametric fashion using the R `cobs` package [12]. Previously, Einmahl and Segers had introduced a compliant non-parametric estimator of the spectral measure that required constrained optimization [17].

The work by Vettori, Huser, and Genton shows that, despite EVC having been studied for a long time, some of the most relevant and accepted methods

fail to meet all the constraints required by the Pickands function even for the bivariate case. Interestingly, semiparametric approaches, like the one introduced by Hernández-Lobato and Suárez for Archimedean copulas [31], have not been explored in the context of EVC as a workable alternative.

We believe that the research community is currently focusing on multivariate extensions and paying less attention to the bivariate case, which is considered a solved problem for all practical purposes with the available tools, some of which have been described above. However, we consider that a more fundamentally sound and general construction is still missing in this context; one for which a large number of parameters can be fit in a fully unconstrained manner without breaking the Pickands function assumptions. The work by Kamnitsi et al. [33] suggests that the bivariate EVC family is not as narrow as could be initially thought by comparison of classical parametric models like those in Table 1, especially if asymmetry treatment is desired. For that matter, we reckon that splines are a powerful tool and the right choice to approximate the Pickands function. Notwithstanding, contrary to other authors, we aim to use them not as a convenient shape-preserving interpolator for non-parametric estimation, but as the core of a semiparametric model like in [31].

A key resource for our investigation has been explored in recent years by the research community, also in the context of Archimedean copulas: the Williamson transform [5]. As we will show in Section 3, from a certain point of view, modelling a Pickands function is similar to modelling an Archimedean generator. McNeil and Nešlehová use the Williamson transform in their study of d -monotone Archimedean generators in [41, 40]. Charpentier et al. also use it pursuing a more general family of multivariate Archimax copulas [10]. As will soon become clear, the work by Fontanari, Cirillo, and Oosterlee, on the use of Lorenz curves as non-strict Archimedean generators, shows that the research community is on the verge of coming at a similar use of the Williamson transform in the context of EVCs.

3 Method

In the following sections we will cover (i) the construction of a new semiparametric EVC, some (ii) convergence and (iii) association results, (iv) its estimation and (v) simulation and, finally, (vi) a possible solution to one of its limitations.

3.1 Construction

Our method addresses both constraints of the Pickands function by geometrically transforming the problem into one for which we know a straight solution.

3.1.1 Affine transformation

First off, the support lines of the Pickands function can be seen as a pair of coordinate axes if conveniently rotated and scaled.

Let M be the unique 2-dimensional affine transformation mapping $(0, 1)$, $(0, 0)$ and $(1, 0)$ to $(0, 1)$, $(1/2, 1/2)$ and $(1, 1)$, respectively. M takes the form

$$M(x, w) = \frac{1}{2} \begin{pmatrix} 1 + x - w \\ 1 + x + w \end{pmatrix}, \quad (18)$$

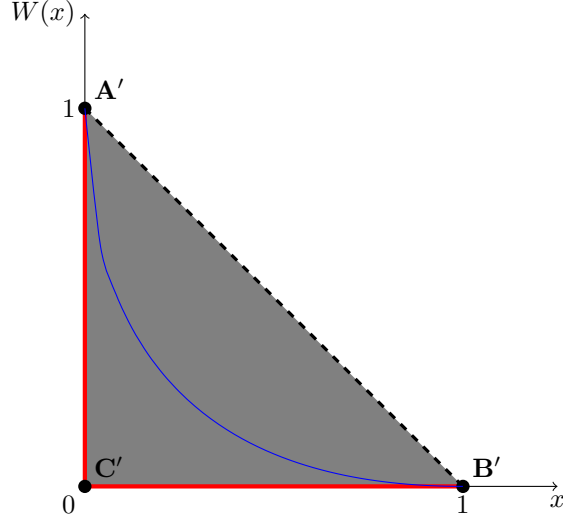


Figure 3: Geometry of a 2-monotone function derived from a Pickands function. The graph of the function W ranges from \mathbf{A}' to \mathbf{B}' and never crosses the line segment between these two points. The rotated version of the Pickands function in Figure 1, $W(x) = x - 2\sqrt{x} + 1$, is drawn in blue.

with inverse

$$M^{-1}(t, a) = \begin{pmatrix} t + a - 1 \\ a - t \end{pmatrix}. \quad (19)$$

Under certain conditions, the inverse mapping M^{-1} transforms the graph of a Pickands function, $\{(t, A(t)) \mid t \in [0, 1]\}$, into the graph of a 2-monotone function W defined on $[0, 1]$ and satisfying $W(0) = 1$ and $W(1) = 0$. Here, 2-monotone stands for non-increasing and convex [41, 10]. Such a W can be more easily modelled than the original Pickands function, as we will see. The transition from one to another is depicted in figures 1 and 3.

Note that for a twice differentiable function W with the above boundary constraints, 2-monotonicity is equivalent to $W'(x) \leq 0$ and $W''(x) \geq 0$, for all $x \in (0, 1)$. This smoothness assumption simplifies the demonstration of the following proposition.

Proposition 1. *Let all the upcoming functions be twice differentiable on $(0, 1)$. By means of (18) and its inverse (19), there is a one-to-one correspondence between Pickands functions A satisfying $A(t) > 1 - t$, for all $t \in (0, 1/2]$, and 2-monotone functions W defined on $[0, 1]$ and satisfying $W(0) = 1$, $W(1) = 0$. Namely, A can be obtained from W as*

$$\begin{cases} t(x) = \frac{1}{2}(1 + x - W(x)) \\ A(t(x)) = \frac{1}{2}(1 + x + W(x)) \end{cases} \quad (20)$$

and conversely, W from A , as

$$\begin{cases} x(t) = t + A(t) - 1 \\ W(x(t)) = A(t) - t \end{cases}, \quad (21)$$

where both $t(x)$ and $x(t)$ are automorphisms of $[0, 1]$.

Proof. Let W be as defined above. We will see that A as defined in (20) is a Pickands function with the additional constraint above.

First, note that $t(0) = 0$, $t(1) = 1$. By continuity of W , this implies that $\text{Ran}(t) = [0, 1]$. Then, for $t(x)$ to be an automorphism of $[0, 1]$, it suffices to see that it is one-to-one. Let us suppose that $t(x_1) = t(x_2)$ for some $x_1, x_2 \in [0, 1]$, $x_1 < x_2$. Then, $W(x_2) - W(x_1) = x_2 - x_1 > 0$, which leads to a contradiction with W being non-increasing. Therefore, $t(x)$ is an automorphism of $[0, 1]$, so A in (20) is well-defined as a function of a single variable $t \in [0, 1]$.

Next, letting the support lines $t_+(x) \equiv t(x)$ and $t_-(x) \equiv 1 - t(x)$, it is easy to check that $t_{\pm}(x) = \frac{1}{2}(1 \pm x \mp W(x))$ and, since both x and $W(x)$ are non-negative (otherwise W would not be non-increasing, with $\text{Ran}(W) = [0, 1]$), we may conclude $A(t(x)) \geq \max\{t_+(x), t_-(x)\}$. Furthermore, $A(t(x)) > 1 - t(x)$ for all $x \in (0, 1] \supset (0, 1/2]$.

Finally, some easy calculations show that

$$A'(t(x)) = \frac{1 + W'(x)}{1 - W'(x)}, \quad (22) \quad A''(t(x)) = \frac{4 W''(x)}{(1 - W'(x))^3}. \quad (23)$$

Since $W'(x) \leq 0$ and $W''(x) \geq 0$, it follows that $A''(t) \geq 0$, for all $t \in (0, 1)$, and hence A is convex. This finishes the proof that (20) defines a Pickands function such that $A(t) > 1 - t$, for all $t \in (0, 1/2]$.

Conversely, let A be a Pickands function with the latter additional constraint. We will similarly show that W as defined in (21) is 2-monotone and satisfies $W(0) = 1$ and $W(1) = 0$.

First, note that $x(0) = 0$ and $x(1) = 0$. By continuity of A , this implies that $\text{Ran}(x) = [0, 1]$. Then, for $x(t)$ to be an automorphism, it suffices to see that $x(t)$ is one-to-one. Let us suppose that $x(t_1) = x(t_2)$ for some $t_1, t_2 \in [0, 1]$, $t_1 < t_2$. This implies that $[A(t_2) - A(t_1)]/(t_2 - t_1) = -1$ and, since A is convex, we must conclude that $A(t) = 1 - t$ for all $t \in (t_1, t_2]$. Clearly, $t_2 \leq 1/2$, because $1 - t < t$ if $t > 1/2$ and, on the other hand, $A(t) \geq \max\{t, 1 - t\}$. Therefore, $(t_1, t_2] \subset (0, 1/2]$, which leads to a contradiction with $A(t) > 1 - t$ over $(0, 1/2]$. Hence, $x(t)$ must be one-to-one and, all in all, an automorphism of $[0, 1]$. This, in turn, means that W in (21) is well-defined as a function of a single variable in $[0, 1]$.

Next, it is easy to check both $W(0) = 1$ and $W(1) = 0$, bearing in mind that $A(0) = A(1) = 1$.

Finally, differentiating in (21), we get, for $t \in (0, 1)$,

$$W'(x(t)) = \frac{A'(t) - 1}{A'(t) + 1}, \quad (24) \quad W''(x(t)) = \frac{2 A''(t)}{(1 + A'(t))^3}. \quad (25)$$

Since $A(t) > 1 - t$ for $t \in (0, 1/2]$ and A being convex, we have $A'(t) > -1$ and the denominator in both (24) and (25) is well-defined. Moreover, $A'(t) \leq 1$, otherwise we would have $A(1 - \epsilon) < 1 - \epsilon$ for a sufficiently small ϵ . Therefore, $W'(x) \leq x$ for all $x \in (0, 1)$. On the other hand, convexity of W follows directly from $A''(t) \geq 0$. \square

Remark 1. *The smoothness assumption in Proposition 1 is not needed in either direction, as we can argue that affine transformations map convex epigraphs into convex epigraphs¹. Hence, the convexity of A is equivalent to that of W . Nonetheless, differentiability is a convenient requirement for our construction, as will become clear in the upcoming sections.*

Let us analyze how some properties of A translate into W .

Proposition 2. *Let A and W be like in Proposition 1.*

1. *A is symmetrical, i.e., $A(t) = A(1 - t)$ for all $t \in [0, 1]$, if and only if W is invertible and $W^{-1} = W$.*
2. *W has a unique fixed point $x^* = x(1/2) = A(1/2) - 1/2$.*
3. *If W is twice differentiable with $W''(x) > 0$, for all $x \in (0, 1)$, and satisfies $W^{-1} = W$, then $W'(x) = -1$ if and only if $x = x^*$, the fixed point.*

Proof. Let us suppose A is symmetrical. First, W must be one-to-one, since $W(x_1) = W(x_2)$ for some $x_1, x_2 \in [0, 1]$, $x_1 < x_2$, would imply, W being non-increasing, that W is constant over $[x_1, x_2]$. Using (21), we get that $A(t) - t$ is constant over $t \in [t_1, t_2] \equiv [t(x_1), t(x_2)]$. That means $A(t) = a + t$ over $[t_1, t_2]$, for some constant $a \in \mathbb{R}$. What is more, since $A(t) > 1 - t$ and A is symmetrical, it turns out that $A(t) > t$ for all $t \in (0, 1)$, thus $a > 0$ necessarily. Now, form the line segment $S(t)$, for $t \in [t_1, 1]$, that satisfies $S(t_1) = A(t_1) = a + t_1$ and $S(1) = A(1) = 1$. It is easy to check that the slope of such an S is $s = (1 - a - t_1)/(1 - t_1)$ and satisfies $0 < s < 1$. Then $S(t_2) = a + t_1 + s(t_2 - t_1) < a + t_2 = A(t_2)$, which contradicts the convexity of A . Therefore, W is one-to-one and has inverse W^{-1} .

Next, to see $W^{-1} = W$, let us start by noting in (21) that the symmetry of A leads to $x(1 - t) = W(x(t))$. Then, applying W to the right side in the latter equation and using it again with argument $1 - t$, we get $W(W(x(t))) = W(x(1 - t)) = x(t)$. Because $x(t)$ is an automorphism, we have $W(W(x)) = x$, for all $x \in [0, 1]$.

Conversely, suppose $W^{-1} = W$. Using $W(W(x)) = x$, straight calculations lead to both $t(W(x)) = t(x)$ and $A(1 - t(x)) = A(t(W(x)))$ and, hence, $A(1 - t(x)) = A(t(x))$, for all $x \in [0, 1]$, so A is symmetrical.

For the second part of the proposition, just note that $W(x(t)) = x(t)$ if and only if $t = 1/2$. Then, substitution of $t = 1/2$ in $x(t)$ yields the expected result.

Finally, for the third part, it is clear that there must exist \tilde{x} such that $W'(\tilde{x}) = -1$. Moreover, as $W'' > 0$, that point must also be unique. Now, since $W^{-1} = W$, the corresponding A is symmetrical. Taking derivatives, $A'(t) = -A'(1 - t) = 0$ if and only if $t = 1/2$. Plugging it into (24), we get $W'(x(1/2)) = -1$, so $\tilde{x} = x(1/2)$, the fixed point from the second part. \square

Using Proposition 2 and (8), we get

$$x^* = \frac{1}{2}(1 - \log_2(1 + \beta)).$$

Therefore, an empirical estimate of β yields a guess at the fixed point of the underlying W .

¹Recall that a function is convex if and only if its epigraph is a convex set.

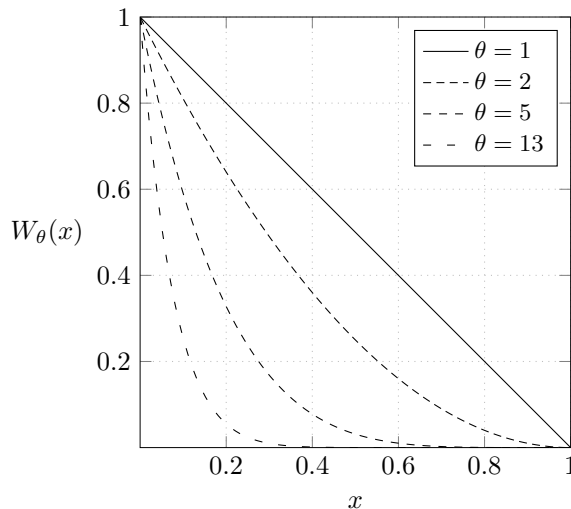


Figure 4: Different instances of the 2-monotone family $W_\theta(x) = (1-x)^\theta$.

Example 2. Elaborating on Example 1, plugging $A(t) = t^2 - t + 1$ into (21) yields the $W(x) = x - 2\sqrt{x} + 1$ we see in Figure 3.

Example 3. The family of functions $W_\theta(x) = (1-x)^\theta$, where $\theta \in [0, \infty)$, meet the conditions in Proposition 1 and thus produce EVCs. They are depicted in Figure 4. Clearly, except for $\theta = 1$, $W_\theta^{-1} \neq W$ and, by Proposition 2, none of them produces an exchangeable EVC.

A W function like the one defined in Proposition 1 induces an spectral measure (11) by means of

$$\eta(z) = \frac{4 W''(t^{-1}(z))}{[1 - W'(t^{-1}(z))]^3} \quad (26)$$

and

$$\mathcal{H}_0 = \frac{2}{1 - W'(0^+)}, \quad (27) \quad \mathcal{H}_1 = \frac{-2W'(1^-)}{1 - W'(1^-)}. \quad (28)$$

Indeed, changing variables and integrating by parts yields

$$\begin{aligned} \int_0^1 z \eta(z) dz &= \int_0^1 t(x) \eta(t(x)) t'(x) dx \\ &= \int_0^1 \frac{[1+x-W(x)] 2W''(x)}{[1-W'(x)]^2} dx \\ &= \left[\frac{1+x-W(x)}{1-W'(x)} \right]_0^1 - 1 \\ &= \frac{1+W'(1^-)}{1-W'(1^-)} \\ &= 1 - \mathcal{H}_1. \end{aligned}$$

Such a W fails to attain the perfect dependence copula, which has Pickands function $A(t) = \max\{1 - t, t\}$. However, it can still model independence if $W(x) = 1 - x$, which yields $A(t) = t \mathcal{H}_0 + (1 - t) \mathcal{H}_1 = t + (1 - t) = 1$.

3.1.2 Williamson transform

The use of W instead of A comes at practically no cost, but it still poses some stringent constraints on derivatives and boundary conditions. However, these are automatically fulfilled if W is the Williamson's transform of a random variable supported on $[0, 1]$ that places no mass at 0.

The Williamson transform had been originally employed in the context of Archimedean copulas as a less restrictive integral transform than Laplace's. Interestingly, McNeil and Nešlehová [41] describe a connection between d -variate Archimedean copulas and d -monotone functions, obtained as Williamson d -transforms of non-negative random variables. Here we will restrict ourselves to the case $d = 2$.

Definition 1. [Williamson transform] Let F be the CDF of a non-negative random variable satisfying $F(0) = 0$. We define the *Williamson transform* of F as

$$\mathfrak{W}\{F\}(x) = \int_x^\infty \left(1 - \frac{x}{r}\right) dF(r).$$

A fundamental result in [41] states that $\Psi = \mathfrak{W}\{F\}$ if and only if Ψ is 2-monotone and satisfies the boundary conditions $\Psi(0) = 1$ and $\Psi(\infty) = \lim_{x \rightarrow \infty} \Psi(x) = 0$. Moreover, such an F is unique and can be retrieved from Ψ as $F(x) = 1 - \Psi(x) + x \Psi'(x^+)$.

It can be easily checked that the support of F is $[0, x^*]$, where $x^* = \inf\{x \in \mathbb{R} \cup \{\infty\} \mid \Psi(x) = 0\}$. In our case, contrary to [41, 10], the support is bounded, since $W(1) = 0$. Therefore, we get the following corollary.

Corollary 1. *A function $W : [0, 1] \rightarrow \mathbb{R}$ is 2-monotone² with $W(0) = 1$ and $W(1) = 0$ if and only if it can be expressed as*

$$W(x) = \int_x^1 \left(1 - \frac{x}{r}\right) dF(r),$$

for some unique CDF F supported on $[0, 1]$ and such that $F(0) = 0$.

Corollary 1 provides a full characterization of functions W in Proposition 1, smoothness assumptions apart, in terms of a much more manageable F , at the cost of an additional integration step. Recall, however, that W and F are equivalent. We can further simplify the construction of W by imposing F be absolutely continuous with probability density function (pdf) f :

$$W(x) = \int_x^1 \left(1 - \frac{x}{r}\right) f(r) dr. \quad (29)$$

The form (29) adds smoothness to W . Differentiating (29) we get

²Non-negative, non-increasing and convex.

$$W'(x) = - \int_x^1 \frac{f(r)}{r} dr, \quad (30) \quad W''(x) = \frac{f(x)}{x}. \quad (31)$$

All in all, the W function satisfies the equation

$$W(x) = \hat{F}(x) + x W'(x), \quad (32)$$

where $\hat{F}(x) = 1 - F(x) = \int_x^1 f$ is the survival function of F . Equation (32) is useful for computational purposes.

From (30) directly follows $W'(1^-) = 0$, thus \mathcal{H}_1 in (28) equals zero. This prevents our method from reaching the independence copula, for which $W(x) = 1 - x$. The value of $W'(0^+)$ (and subsequently of \mathcal{H}_0) is, however, dependant on the behaviour of f near 0.

Example 4. Expanding on Example 2, by using (31), we find that $F(x) = \sqrt{x}$. Hence, F is the CDF of U^2 , where $U \sim \text{Unif}[0, 1]$.

Example 5. Elaborating on Example 3, if $\theta > 1$, by (31), we get $f(x) = \theta(\theta - 1)x(1 - x)^{\theta-2}$, which is the pdf of the Beta($\alpha = 2, \beta = \theta - 1$) distribution.

Example 6. Example 4 is a special case of Williamson transforms of positive³ powers U^θ of the uniform distribution on $[0, 1]$. The general formulas for their densities and CDFs are

$$f_{U^\theta}(x) = \frac{1}{\theta} x^{\frac{1}{\theta}-1}, \quad (33)$$

and $F_{U^\theta}(x) = x^{\frac{1}{\theta}}$, respectively, whereas their Williamson transform is given by

$$W_{U^\theta}(x) = \begin{cases} 1 + \frac{1}{\theta-1}x - \frac{\theta}{\theta-1}x^{\frac{1}{\theta}}, & \text{if } \theta \neq 1 \\ 1 - x + x \log x, & \text{if } \theta = 1 \end{cases}. \quad (34)$$

All $W_\theta \equiv W_{U^\theta}$ in (34) are twice differentiable with $W_\theta''(x) > 0$. For Proposition 2, if any W_θ is to satisfy $W_\theta^{-1} = W_\theta$, then it must also satisfy $W_\theta'(\tilde{x}) = -1$, where \tilde{x} is the unique fixed point, for which $W_\theta(\tilde{x}) = \tilde{x}$. Considering both equations, one can check that the assumption $\theta \neq 2$ leads to a contradiction, which proves $\theta = 2$ is the only case where the Williamson transform yields an exchangeable copula. Figure 5 shows several instances of this family.

At this point, any n -parameter univariate pdf family $\{f_\theta \mid \theta \in \mathbb{R}^n\}$ yields an equivalent n -parameter EVC family by integrating (29) and affinely transforming (20). However, the final target of our method are semiparametric models, where n is expected to become large. In order to introduce such models we need to introduce further simplification and additional approximation techniques.

3.1.3 Bayes space

For modelling f we will turn to the Hilbert space of probability density functions [16, 37]. Consider the set \mathcal{P} of all probability density functions f supported on $[0, 1]$, i.e., non-negative functions with $\int_0^1 f = 1$, and such that there exist m and M satisfying $0 < m \leq f(x) < M$ for all $x \in [0, 1]$. Then, letting $f, g \in \mathcal{P}$ and $\alpha \in \mathbb{R}$, consider the addition and scalar multiplication operations

³For $\theta \leq 0$, the resulting random variable is not bounded.

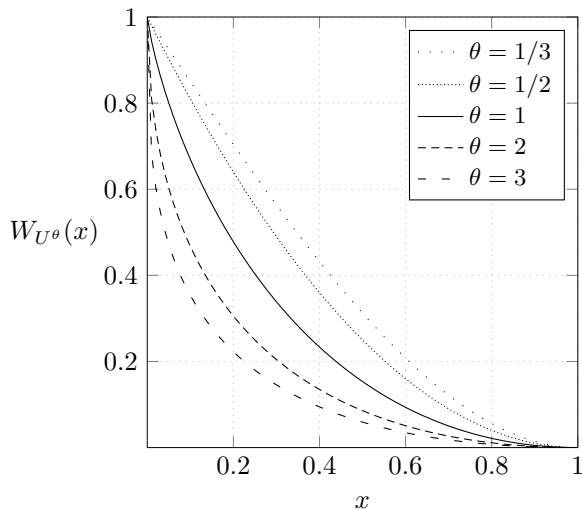


Figure 5: Different instances of the 2-monotone family (34). Values $\theta < 1$ produce finite slopes at 0^+ . The case $\theta = 2$ yields $W_{U^2}(x) = x - 2\sqrt{x} + 1$, the only member of the family that is its own inverse. The case $\theta = 1/2$ coincides with the case $\theta = 2$ in Figure 4 and Example 5.

$$(f \oplus g)(x) = \frac{f(x)g(x)}{\int_0^1 f(y)g(y) dy}, \quad (\alpha \odot f)(x) = \frac{f(x)^\alpha}{\int_0^1 f(y)^\alpha dy}.$$

Finally, consider the inner product

$$\langle f, g \rangle_{\mathcal{B}^2} = \frac{1}{2} \int_{[0,1]^2} \log \frac{f(x)}{f(y)} \log \frac{g(x)}{g(y)} dx dy. \quad (35)$$

Endowed with all these elements and after completion, $\mathcal{B}^2 = (\mathcal{P}, \oplus, \otimes, \langle \cdot, \cdot \rangle)$ is the Hilbert space [16] of square-integrable logarithm, where the null elements corresponds to the uniform density, $\text{Unif}[0, 1]$. This construction is the continuous counterpart of Aitchison geometry [16]. The space \mathcal{B}^2 is known as the Bayes space, because of the resemblance of the Bayesian update rule $p(\theta|x) \propto p(x|\theta)p(\theta)$ with the perturbation operator \oplus .

In what follows, we shall use the above operations indistinctly with probability density functions, distributions or random variables.

As defined, functions in \mathcal{P} are strictly positive and bounded, which would make both Example 4 and Example 5 unreachable. Additionally, now we definitely have $W'(0^+) = -\infty$ and $\mathcal{H}_0 = 0$ in (27). Therefore, the spectral measure induced by such an f would be absolutely continuous with respect to the Lebesgue measure on $[0, 1]$ with Radon-Nikodym derivative equal to (26).

The space \mathcal{B}^2 can be injected into $L^2([0, 1])$ by means of the centered log-ratio transformation

$$\text{clr}[f](x) = \log f(x) - \int_0^1 \log f(y) dy. \quad (36)$$

However, note that not every element in $L^2([0, 1])$ is attainable, since (36) introduces the constraint $\int_0^1 \text{clr}[f] = 0$. If we define the subspace $L_0^2([0, 1])$ of the functions with zero integral, then (36) is a bijection from \mathcal{B}^2 to $L_0^2([0, 1])$ with inverse

$$\text{clr}^{-1}[p](x) = \frac{\exp p(x)}{\int_0^1 \exp p(y) dy}. \quad (37)$$

What is more, (36) is an isometry between \mathcal{B}^2 and $L_0^2([0, 1])$, since calculations show that

$$\text{clr}[f \oplus g] = \text{clr}[f] + \text{clr}[g], \quad (38) \quad \text{clr}[\alpha \odot f] = \alpha \text{clr}[f], \quad (39)$$

$$\langle f, g \rangle_{\mathcal{B}^2} = \langle \text{clr}[f], \text{clr}[g] \rangle_{L^2}. \quad (40)$$

Example 7. The densities of positive powers U^θ of the uniform distribution (33) have centered log-ratio transforms

$$\text{clr}[U^\theta](x) = \frac{1 - \theta}{\theta} (1 + \log x). \quad (41)$$

From this immediately follows that all U^θ are linearly dependent, i.e., given any $\beta \neq 1$, any other $\alpha > 0$ can be expressed as

$$U^\alpha = \frac{\beta(1 - \alpha)}{\alpha(1 - \beta)} \odot U^\beta.$$

Example 8. The mirrored version $1 - U^\theta$ of (33) can also be considered, but this time its Williamson transform has no simple closed form. Notwithstanding, it can be checked that

$$\text{Beta}(\alpha, \beta) = U^{\frac{1}{\alpha}} \oplus (1 - U^{\frac{1}{\beta}}), \quad \alpha, \beta \in (0, \infty).$$

All Beta distributions can be expressed in the centered log-ratio space as

$$\lambda_1 \log ex + \lambda_2 \log e(1 - x) \text{ for some } \lambda_1, \lambda_2 \in \mathbb{R}.$$

By means of the isometry (37) we can search for a suitable function in $L_0^2([0, 1])$, where the usual notions of sum, scalar multiplication and inner product stand, and then transform it back to a pdf. However, this space is infinite-dimensional, thus in practice we shall work on a finite subspace. Example 8 provides a premier example on a 2-dimensional subspace, spanned by $\log ex$ and $\log e(1 - x)$. In general, we will build a pdf $f_\theta(x)$ as a linear combination

$$f_\theta(x) = \bigoplus_{i=1}^n (\theta_i \odot \text{clr}^{-1}[\varphi_i])(x) = \text{clr}^{-1} \left[\sum_{i=1}^n \theta_i \varphi_i(x) \right], \quad (42)$$

where we can assume the $(\varphi_i)_{i=1}^n$ are orthonormal, i.e. $\langle \varphi_i, \varphi_j \rangle_{L^2([0,1])} = \delta_{ij}$, and satisfy the zero-integral constraint.

Any finite-dimensional subspace can also be seen as a statistical manifold [18] from information geometry. Densities behave like vectors and can be

added (perturbed) and scaled (powered). At the same time, they can be viewed as tuples of coordinates, in which this operation does not necessarily apply. The geometry induced by (40) is flat, in the sense that the metric tensor δ_{ij} is constant. From the perspective of information geometry, at each f_{θ} there exists a metric tensor field defined by

$$I_{ij}(\theta) = \mathbb{E}[\varphi_i(X) \varphi_j(X)] - \mathbb{E}[\varphi_i(X)] \mathbb{E}[\varphi_j(X)], \text{ where } X \sim f_{\theta}, \quad (43)$$

and known as the Fisher information metric. Note that taking $X \sim \text{Unif}[0, 1]$ above we retrieve the constant metric tensor δ_{ij} from the Aitchison geometry [18]. In that sense, it could be argued that Aitchison geometry places a reference density at all points of the manifold, which coincides with the null element $f_{\mathbf{0}}$.

For the purpose of our method, the use of the Fisher metric (43) is not fully relevant. This metric defines the local geometry of the statistical manifold of the $\{f_{\theta}\}$, but these vectors are just a mean to model EVCs; we have no interest in them from an information-theoretic perspective. If we were to model univariate distributions in the Bayes space, the Fisher metric could be used for regularization and optimization purposes.

The null element $f_{\mathbf{0}} \sim \text{Unif}[0, 1]$ produces the Williamson transform (34) for $\theta = 1$. The resulting Pickands function after rotation (20) has an explicit form that involves the Lambert W function [11], which cannot be expressed in terms of elementary functions and needs to be numerically approximated. Should the parameters in (42) be normally distributed with zero mean vector, we would expect the Pickands function to lie close to the graph in Figure 6. In this sense, our method presents a very slight bias towards asymmetry.

The asymmetry bias can be corrected if we consider an affine subspace instead of a pure vector space, using a convenient $\omega \in L^2([0, 1])$ as center:

$$f_{\theta} = \text{clr}^{-1}[\omega] \oplus \bigoplus_{i=1}^n (\theta_i \odot \text{clr}^{-1}[\varphi_i]). \quad (44)$$

3.1.4 Compositional splines

Machalová et al. in [37] formalize the construction of a spline basis that meets the zero integral constraint. The resulting splines are called ZB-splines and can be efficiently computed as a linear combination of the usual B-splines. We refer the reader to [37] for further details on how to compute ZB-splines and to [6] for deeper knowledge on B-splines, in general.

Given $0 = \kappa_0 < \kappa_1 < \dots < \kappa_{n+1} = 1$, where $n \geq 0$, and assuming $2d$ additional coincidental⁴ knots $\kappa_{-d} = \dots = \kappa_{-1} = 0$ and $\kappa_{n+1} = \dots = \kappa_{n+d+1} = 1$ at the endpoints, the space of splines $p \in \mathcal{Z}_{\kappa}^d$ of degree less than or equal to d and $n + 2$ different knots $\kappa = (\kappa_i)_{i=0}^{n+1}$ has dimension $n + d$. The case $n = 0$, corresponds to zero-integral polynomials over $[0, 1]$. Altogether, any zero-integral spline can be expressed as

$$p_{\theta}(x) = \sum_{i=1}^{n+d} \theta_i Z_i(x), \text{ for } \theta = (\theta_1, \dots, \theta_{n+d}) \in \mathbb{R}^{n+d}, \quad (45)$$

⁴Coincidental knots at the interval endpoints convey maximum smoothness at each interior knot [6]. For splines of degree less than or equal to d , we have $d - 1$ continuous differentiability everywhere in $[0, 1]$.

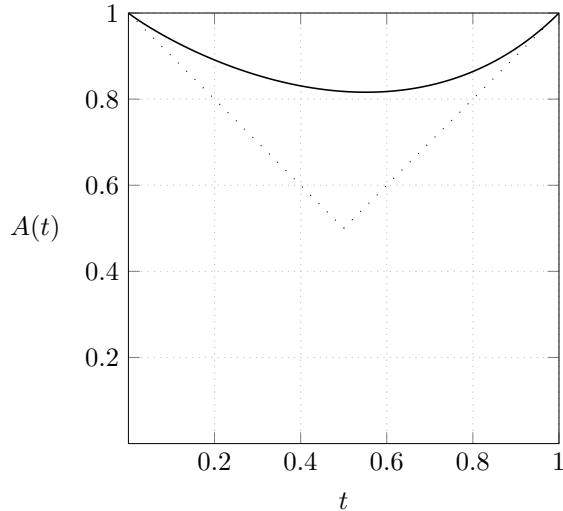


Figure 6: Pickands function $A(t) = 1 - t + \exp\{\mathcal{W}_{-1}(-2t/e^2) + 2\}$ arising from the Williamson family (34) for $\theta = 1$. Here \mathcal{W}_{-1} denotes the $k = -1$ branch of the complex Lambert W function.

where $\int_0^1 Z_i = 0$ and we can further assume an orthonormal basis [37], i.e., $\langle Z_i, Z_j \rangle_{L^2} = \delta_{ij}$. As $\mathcal{Z}_\kappa^d \simeq \mathbb{R}^{n+d}$, given $p_{\theta_1}, p_{\theta_2} \in \mathcal{Z}_\kappa^d$, we have $\langle p_{\theta_1}, p_{\theta_2} \rangle_{L^2} = \langle \theta_1, \theta_2 \rangle_{\mathbb{R}^{n+d}} = \theta_1 \cdot \theta_2$, the canonical dot product.

Furthermore, we can place a convenient center for our ZB-spline space, so that the asymmetry bias is corrected. We propose to take $\omega(x)$ in (44) to be the orthogonal projection $z(x)$ of $-\frac{1}{2}(1 + \log x)$, the case $\theta = 2$ in (41), onto the space (45)

$$z(x) = \sum_{i=1}^{n+d} \langle \text{clr}[U^2], Z_i \rangle_{L^2} Z_i(x). \quad (46)$$

This way, the resulting zero-integral function remains a spline in the original basis and thus coordinates may be updated by simply adding at each component the correspondent $\langle \text{clr}[U^2], Z_i \rangle_{L^2}$ projection. Figure 7 shows that the logarithmic center can be effectively approximated by a spline, despite the divergence near zero. The effectiveness of the bias correction is illustrated in Figure 8. The underlying orthonormal ZB-spline basis $\{Z_i\}$ is depicted in Figure 9.

From a practical standpoint, (45) can be directly used in a MCMC simulation [22] to draw samples from the corresponding distribution, since $p_\theta = \log f_\theta + K$, for some constant $K \in \mathbb{R}$ that eventually cancels out.

3.2 Convergence

On this section we will present some basic results on how convergence on the Bayes space relates to convergence for the resulting extreme-value copulas through our method.

Let us first recall the definition of the supreme norm of a bounded function $f : \mathcal{X} \rightarrow \mathbb{R}$, which will be used to measure distances between some objects we

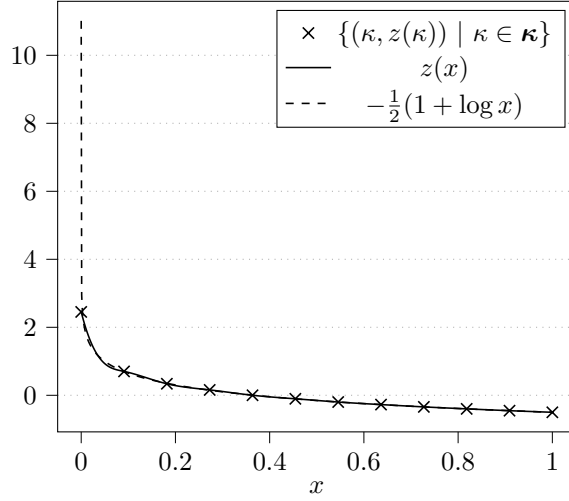


Figure 7: Projection $z(x)$ of $-\frac{1}{2}(1 + \log x)$ onto an orthonormal ZB-spline 13-dimensional basis with knots κ . The logarithmic function diverges to infinity at 0.

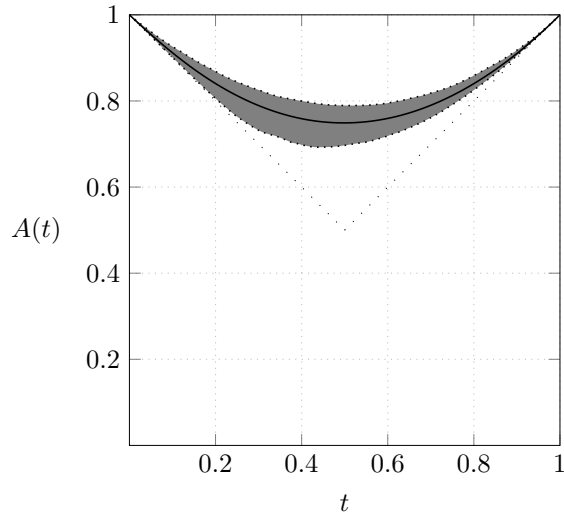


Figure 8: Random Pickands functions built as perturbations around center (46). Namely, all θ_i were sampled from a normal distribution with zero mean and $\sigma = 0.1$. A total of 1000 Pickands functions were randomly drawn. The solid line represents the mean function, while the grey envelope represents the confidence interval between quantiles 1% and 99%. The mean line is close to the $A(t) = t^2 - t + 1$ in Figure 1.

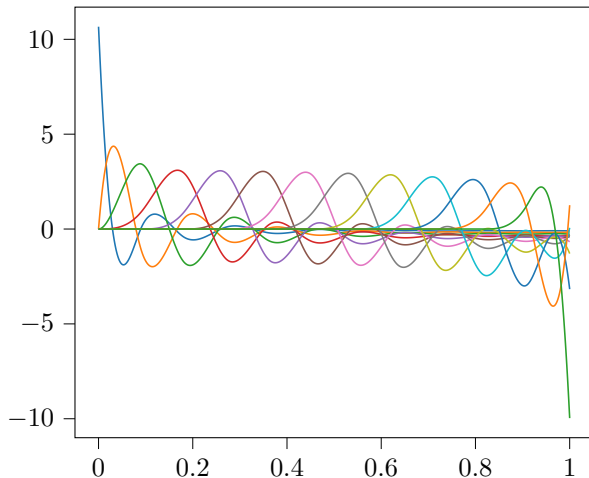


Figure 9: Orthonormal cubic ZB-spline basis with 13 elements.

have previously introduced:

$$\|f\|_\infty = \sup_{x \in \mathcal{X}} |f(x)|. \quad (47)$$

On this paper, \mathcal{X} will typically be a compact subset of \mathbb{R}^n , namely $[0, 1]$, for functions W and A , and $[0, 1]^2$, for copulas C . The norm (47) defines a distance $d_\infty(f, g) = \|f - g\|_\infty$. A sequence of functions $\{f_n\}_{n=1}^\infty$ converging on the latter distance to some f is said to converge *uniformly*. A nice property of uniform convergence is that such an f is necessarily continuous.

Sometimes, however, uniform convergence is a rather strong property to be realistically achieved. For instance, the function f may not be bounded on the whole \mathcal{X} . In those cases, a more subtle convergence exists, only requiring the sequence converging uniformly to f on every compact subset \mathcal{K} of \mathcal{X} . Then, the sequence of $\{f_n\}_{n=1}^\infty$ is said to be *compactly convergent* to f .

Another related concept can be applied to probability measures.

Definition 2. Let \mathbb{P} and \mathbb{Q} be probability measures on the space $[0, 1]$ equipped with the Borel σ -algebra \mathcal{B} . The *total variation distance* (TVD) between \mathbb{P} and \mathbb{Q} is defined as

$$d_{\text{TV}}(\mathbb{P}, \mathbb{Q}) = \sup_{B \in \mathcal{B}} |\mathbb{P}(B) - \mathbb{Q}(B)|. \quad (48)$$

TVD satisfies all three axioms of a true metric. By Scheffé's theorem [51], it can also be expressed in terms of the pdf f and g of \mathbb{P} and \mathbb{Q} , respectively, as

$$d_{\text{TV}}(\mathbb{P}, \mathbb{Q}) \equiv d_{\text{TV}}(f, g) = \frac{1}{2} \int_0^1 |f(x) - g(x)| dx. \quad (49)$$

Our first result links convergence in total variation of a sequence of pdfs with convergence of the corresponding sequence of Williamson's transforms and their derivatives.

Proposition 3. Let $\{f_n\}_{n=1}^\infty$ be a sequence of pdfs supported on $[0, 1]$ such that $\lim_{n \rightarrow \infty} d_{\text{TV}}(f, f_n) = 0$ for some pdf f also on $[0, 1]$. Let W_n and W be the

corresponding Williamson's transforms of f_n and f , respectively. Then, the sequence $\{W_n\}_{n=1}^\infty$ uniformly converges to W on $[0, 1]$. Moreover, $\{W'_n\}_{n=1}^\infty$ compactly converges to W' on $(0, 1]$.

Proof. It suffices to check that, for all $x \in [0, 1]$,

$$|W(x) - W_n(x)| = \left| \int_0^1 \left(1 - \frac{x}{r}\right)_+ [f(r) - f_n(r)] dr \right| \leq \int_0^1 |f(r) - f_n(r)| dr,$$

where $(\cdot)_+$ denotes the non-negative part of the argument, and then apply Scheffé's theorem (49). Similarly, considering the compact subset $[x_0, 1]$, for some $x_0 > 0$, we have, for all $x \in [x_0, 1]$,

$$|W'(x) - W'_n(x)| \leq \frac{2}{x_0} d_{\text{TV}}(f, f_n).$$

□

For instance, taking $W_n(x) = (1 - x)^n$ from Example 3, it is easy to check that, as $n \rightarrow \infty$, W_n approaches the indicator function on $x = 0$, which is discontinuous at that point and, hence, $\{W_n\}_{n=1}^\infty$ does not converge uniformly. For Proposition 3, the underlying sequence $f_n(x) = n(n - 1)x(1 - x)^{n-2}$ in Example 6 cannot be convergent in total variation. Indeed, the limiting distribution of the latter Beta distributions is a degenerate Dirac Delta at $x = 0$, thus the limit has no pdf. Nonetheless, even omitting the pdf requirement, the TVD would be equal to 1. To see this, consider in (48) the Borel set $B = \{0\}$ consisting solely of the degenerate point $x = 0$. Then, all the Beta distributions place zero probability on B , but the Dirac Delta does the opposite, as $\delta_0(\{0\}) = 1$. Note, however, that even though the premises of Proposition 3 are not met, $\{W'_n\}_{n=1}^\infty$, with $W'_n(x) = n(1 - x)^{n-1}$, compactly converges to $W'(x) = 0$ over $(0, 1]$.

The next step links uniform convergence of Williamson's transforms with that of Pickands functions. To be fair, uniform convergence of pointwise-convergent sequences of Pickands functions can be established by other means, as pointed out in [20]. Notwithstanding, the next result also states the uniform convergence of the first derivatives of Pickands functions under the same hypotheses, which cannot be taken for granted.

Proposition 4. *Let $\{W_n\}_{n=1}^\infty$ be a sequence of Williamson transforms, arising from pdfs, uniformly convergent to some other Williamson transform W on $[0, 1]$. Also, suppose the sequence of first derivatives $\{W'_n\}_{n=1}^\infty$ of the previous functions compactly converge to W' on $(0, 1]$. Let A_n and A be the corresponding Pickands functions of W_n and W , respectively, according to our method. Then, the sequence $\{A_n\}_{n=1}^\infty$ uniformly converges to A on $[0, 1]$, while $\{A'_n\}_{n=1}^\infty$ compactly converges to A' on $(0, 1]$.*

Proof. It follows from the equivalence between uniform convergence and function graph convergence [53] for functions with compact domain and range. Since the W_n 's uniformly converge to a continuous function W , the sequence of the graphs of the W_n 's has its limit in the graph of W . Then, note that the graphs of A_n and A are affine transformations (20) of the graphs of W_n and W , respectively, which ensures, by continuity, that the graphs of the A_n 's tend to that of A . Finally, graph convergence for the A_n 's implies uniform convergence to A itself.

The result for the first derivatives follows similarly. This time, instead of an affine map, the functions mapping the graph of W to that of A and vice versa are, respectively,

$$\mathbb{T} : (x, w) \mapsto \left[t(x), \frac{1+w}{1-w} \right], \quad \mathbb{X} : (t, a) \mapsto \left[x(t), \frac{a-1}{a+1} \right].$$

Both are the inverse of one another, because of (22) and (24). Clearly, both functions are continuous, thus they preserve compactness and graph convergence.

To see that $\{A'_n\}_{n=1}^\infty$ compactly converges to A' , consider any compact set $\mathcal{K} = [t_0, 1]$, for $t_0 > 0$. Then, consider the sequence of restricted function graphs $\{\mathcal{G}[A'_n|_{\mathcal{K}}]\}_{n=1}^\infty$ and apply \mathbb{X} to every element to obtain another sequence $\{\mathcal{G}[W'_n|_{\mathbb{X}(\mathcal{K})}]\}_{n=1}^\infty$. Now, $\mathbb{X}(\mathcal{K})$ is a compact set, so $W'_n|_{\mathbb{X}(\mathcal{K})}$ uniformly converges to $W'|_{\mathbb{X}(\mathcal{K})}$ and, because of [53], the graph sequence approaches $\mathcal{G}[W'|_{\mathbb{X}(\mathcal{K})}]$. The argument finishes by noting that, since \mathbb{T} is continuous and since $\mathbb{T}(\mathcal{G}[W'_n|_{\mathbb{X}(\mathcal{K})}]) = \mathcal{G}[A'_n|_{\mathcal{K}}]$ and $\mathbb{T}(\mathcal{G}[W'|_{\mathbb{X}(\mathcal{K})}]) = \mathcal{G}[A'|_{\mathcal{K}}]$, the graphs of the $A'_n|_{\mathcal{K}}$'s tend to that of $A'|_{\mathcal{K}}$. \square

Remark 2. *Uniform convergence of function derivatives is mostly unconnected to uniform convergence of the functions themselves. The reason why it works in this case comes down to the form of the Williamson's transform, whose first derivative is also in a convenient integral transform that allows to apply total variation convergence of the internal pdfs to both the function and its derivative, at the same time.*

The uniform convergence of copulas can be established on topological grounds from pointwise convergence [46]. Notwithstanding, there exists a connection between the supreme norms of copulas and that of their respective Pickands function [33]. Namely, $\|C_1 - C_2\|_\infty \leq 2\gamma/(1 + 2\gamma)^{1+1/(2\gamma)}$, where $\gamma = \|A_1 - A_2\|_\infty$.

We turn next to some assumptions making convergence in $L_0^2([0, 1])$ sufficient for pdfs to converge uniformly.

Proposition 5. *Let $\{p_n\}_{n=1}^\infty \subset L_0^2([0, 1])$ continuous and uniformly bounded, i.e., $\|p_n\|_\infty \leq K$ for some $K > 0$ and for all n . Suppose $\lim_{n \rightarrow \infty} \|p - p_n\|_2 = 0$, for some $p \in L_0^2([0, 1])$. Let $f_n = \text{clr}^{-1}[p_n]$ and $f = \text{clr}^{-1}[p]$. Then, $\lim_{n \rightarrow \infty} d_{TV}(f, f_n) = 0$.*

Proof. First, note that continuity ensures that the limit p is also bounded by the same K . Denoting $I_q = \int_0^1 e^q$, some easy calculations show that

$$|f(x) - f_n(x)| \leq \frac{e^{p(x)}|I_p - I_{p_n}| + I_p |e^{p(x)} - e^{p_n(x)}|}{I_p I_{p_n}}.$$

Now, the integrals are bounded, namely $e^{-K} \leq I_q \leq e^K$. On the other hand, $|e^{p(x)} - e^{p_n(x)}| \leq e^K |p(x) - p_n(x)|$, using the *mean value theorem* and the fact that both functions are bounded by K . Altogether,

$$|f(x) - f_n(x)| \leq e^{4K} \left(\int_0^1 |p(y) - p_n(y)| dy + |p(x) - p_n(x)| \right).$$

Integrating both sides of the last inequality and using Jensen's inequality, we finally get

$$d_{\text{TV}}(f, f_n) \leq e^{4K} \|p - p_n\|_1 \leq e^{4K} \|p - p_n\|_2$$

□

Altogether, our method, acting on convergent sequences in $L_0^2([0, 1])$, produces EVCs that not only uniformly converge, but also whose partial derivatives do.

Corollary 2. *Let $\{z_n\}_{n=1}^\infty \subset L_0^2([0, 1])$ be a sequence of uniformly bounded smooth cubic ZB-splines that converge in the $\|\cdot\|_2$ norm. The corresponding EVCs from our method $\{C_n\}_{n=1}^\infty$ uniformly converge to some EVC C , satisfying, for $i = 1, 2$,*

$$\partial_i C_n \xrightarrow[n \rightarrow \infty]{\|\cdot\|_\infty} \partial_i C \text{ compactly over } (0, 1]^2.$$

Proof. It follows from all the previous convergence results and from the examination of (7), where all the terms in the right-hand side uniformly converge on compact sets. □

3.3 Association measures

As mentioned earlier, Kendall's tau and Spearman's rho, two of the most well-known measures of association between two random variables, depend solely on the copula linking the two. In the case of an EVC, both measures can be expressed as integrals involving the Pickands function [33]. The substitution of the Pickands function by the equivalent functional form of the Williamson transform and a change of variables afterwards do not provide any meaningful insight on the role played by the latter. However, the apparent relation between Williamson transforms and Lorenz curves reveals a new path for measuring association.

The Williamson form W of a Pickands function A satisfies the definition of a Lorenz [21] curve L after the change of variable $L(x) = W(1 - x)$, for $x \in [0, 1]$. Lorenz curves are employed in economics for assessing wealth inequality, for which an index can be derived, known as the Gini coefficient:

$$G = 1 - 2 \int_0^1 L.$$

The G index has a geometrical interpretation as the area between L and $x \mapsto x$ divided by the area under $x \mapsto x$, which is equal to $1/2$. The same interpretation applies to W and, since $\int_0^1 W = \int_0^1 L$, we have $G = 1 - 2 \int_0^1 W$. A value of $G = 0$ means wealth is uniformly distributed (the $p\%$ wealthiest proportion of the population accumulate $p\%$ of the total wealth, for all $p \in [0, 1]$), whereas $G \lesssim 1$ means that nearly all wealth is concentrated on a tiny fraction of the population. In summary, $G = 0$ represents perfect equality, while $G = 1$ represents perfect inequality.

Now, in our context, a Pickands function A is just the affine transformation of some W . Since affine transformations change areas by applying a constant factor, the latter cancels out in ratio measures, leaving them invariant. Therefore, the Gini coefficient can be restated in terms of A as the area between A

and the upper bound line $\{y = 1\}$ divided by the area between the support lines and the upper bound line. This argument leads to

$$G = 4 \left(1 - \int_0^1 A \right). \quad (50)$$

The value $G = 1$ is attained when A is identically equal to the lower support lines ($\int_0^1 A = 3/4$), producing the perfect dependence copula. On the other hand, $G = 0$ is attained when A is identically equal to the upper bound line ($\int_0^1 A = 1$), producing the independence copula. This way, bivariate positive association can be interpreted in economic terms: perfect dependence is equivalent to perfect inequality, whereas independence corresponds to perfect equality.

The Gini coefficient is not a common association measure in the context of EVCs, despite its simplicity. In fact, we have only found a brief mention to a slightly modified version of it in [30], where the measure was not scaled to lie on $[0, 1]$ and Pickands symmetry was further assumed. The index can be reformulated for any *positively quadrant dependent* copula C , i.e., $C(u, v) \geq uv$, for all $u, v \in [0, 1]^2$, as⁵

$$G = 4 \left(1 - \int_{[0,1]^2} \frac{\log C(u, v)}{\log uv} dudv \right). \quad (51)$$

The Gini coefficient, as defined above, satisfies the axioms of a *dependence measure* [7], taking values on $[0, 1]$, unlike Kendall's tau and Spearman's rho, that belong to a more general family of *concordance measures*, ranging in $[-1, 1]$ and allowing for negative association. Although we call it Gini coefficient, because of its origin, it is not to be confused with another well-known concordance measure: Gini's gamma.

Interestingly for our method, the area of W can be expressed in terms of the inner density f , after integrating by parts twice, yielding

$$G = 1 - \mathbb{E}[X], \text{ where } X \sim f. \quad (52)$$

Equation (52) links a complex integral calculation in two dimensions (51) to a much simpler one, which can even be approximated by MCMC simulation only evaluating the underlying zero-integral $\text{clr}[f]$.

Example 9. The EVC family defined in Example 5 has a wide range of Gini coefficient values, in terms of a parameter $\theta \in [1, \infty)$, as $G = (\theta - 1)/(\theta + 1)$.

Example 10. The EVC family defined in Example 6 also has a wide range of Gini coefficient values, in terms of a parameter $\theta \in (0, \infty)$, as $G = \theta/(\theta + 1)$.

3.4 Estimation

The estimation process builds upon the various constructions explored above. Given an orthonormal ZB-spline basis, we aim to find the parameter vector $\boldsymbol{\theta}$ that best fits a dataset. Starting from a zero-integral spline (42) $p_{\boldsymbol{\theta}}$, we apply the inverse centered log-ratio transformation (37) to obtain a pdf $f_{\boldsymbol{\theta}}$ over $[0, 1]$. Then, we integrate the pdf using the Williamson transform (29) to obtain a

⁵The CDF (16) and its stochastic interpretation provide a shortcut to check this.

2-monotone function W_{θ} . Finally, we rotate that function to get to the targeted Pickands function A_{θ} , using (20). Once arrived at the Pickands function, the construction of the EVC follows from the definition (6).

Knowing the one-to-one relation [8] between the random vector (U, V) following an EVC and the random variable $Z = \log U / \log(UV)$, we reduce our problem to fitting the latter, which has a simpler density, straightly derived from (16):

$$h(z) = 1 + (1 - 2z) \frac{A'(z)}{A(z)} + z(1 - z) \left[\frac{A''(z)}{A(z)} - \left(\frac{A'(z)}{A(z)} \right)^2 \right]. \quad (53)$$

Clearly, the corresponding \tilde{h} density for the symmetrical counterpart \tilde{A} of A is $z \mapsto h(1 - z)$. Therefore, A will be symmetrical if and only if h is symmetrical around the $\{z = 1/2\}$ axis.

Given a random sample $\mathcal{D} = \{z_i\}_{i=1}^m$ from Z and a model h_{θ} derived from p_{θ} up to A_{θ} , the frequentist approach to the estimation addresses the maximization of the penalized log-likelihood of h_{θ}

$$\ell(\theta|\mathcal{D}) = \sum_{i=1}^m \log h_{\theta}(z_i) - \lambda \int_0^1 (p_{\theta}'')^2, \quad (54)$$

for some regularization hyper-parameter $\lambda \geq 0$. The square norm term involving p_{θ}'' is the linearized curvature of the spline: a simplified non-intrinsic form of the curvature that can be expressed as a covariant tensor $\theta^T \Omega \theta$, where $\Omega = (\Omega_{ij}) = (\int_0^1 Z_i'' Z_j'')$. As can be seen from Figure (9), especially if the dimension of the basis is large, splines may exhibit complex shapes prone to overfitting. Penalizing the curvature is the proposed method in [37] in the context of compositional data regression, but has also been successfully applied in semiparametric copula models [31]. For $\lambda = 0$, regularization is turned off, retrieving the usual log-likelihood.

From a Bayesian perspective, maximizing (54) is equivalent to obtaining the maximum a posteriori (MAP) estimator of θ from dataset \mathcal{D} applying an exponentially distributed prior on the spline curvature with rate parameter λ . In the Bayesian approach we can more generally analyze the distribution of θ to assess multimodality and variability and, overall, the posterior mean is preferred to the MAP estimator.

Estimating the parameters of such a model poses some important challenges. First and foremost, the evaluation alone of the resulting Pickands function from a parameter vector and a single argument implies several non-trivial operations, most notably the integral and affine transformations (29) and (20), respectively. Although they can be accurately applied, from a numerical standpoint, they are time-consuming, which may hinder the overall estimation process. Therefore, we propose key approximations at each step.

First, note that the evaluation of A in (20) at a specific value t_0 requires solving for x in $t(x) = t_0$. The latter will be generally a nonlinear equation that can only be solved through numerical methods, at a relatively high computational cost. Hence, in most cases, evaluating (53) in (54) at each point z_i becomes rapidly unaffordable as m increases. What is more, any root finding procedure of our choice would prevent us from applying gradient optimization, as it would stop backpropagation. Taking all into consideration, we propose

to approximate h_{θ} by a linear interpolator \tilde{h} with sufficiently numerous and carefully selected knots.

Since (54) is based on an empirical univariate sample \mathcal{D} , a reasonable knot selection utilizes uniform quantiles of \mathcal{D} , thus knots will be more separated on low probability regions and will accumulate on high probability ones. This criterion, which was employed on a similar setting in [31], reduces the variance of the parameter vector θ . Once fixed the quantiles $\{q_i\}_{i=1}^k$, we need to estimate some $\{x_i\}_{i=1}^k$ such that $t_i \equiv t_{\theta}(x_i) \approx q_i$ and then take $h_i = h_{\theta}(t_i)$ as the linear interpolator value at knot t_i . Note that the t_i 's are just approximations for the q_i 's. To estimate the required x_i 's, we may apply (21) over the q_i 's grid using an empirical nonparametric estimate of the Pickands function, like (17). The procedure can be stated as follows.

Algorithm 1. Let $\mathcal{D} = \{z_i\}_{i=1}^m$ be a random sample following the H distribution. To build an interpolation grid $\{x_i\}_{i=0}^{k+1}$ in the W_{θ} space such that $\{t_{\theta}(x_i)\}_{i=0}^{k+1}$ are roughly distributed according to \mathcal{D} , follow these steps:

1. Pick k uniform quantiles $0 = q_0 < q_1 < \dots < q_{k+1} = 1$ of \mathcal{D} .
2. Build the empirical CDF \tilde{H} of \mathcal{D} .
3. Build an empirical estimate \tilde{A} using \tilde{H} and (17).
4. Set $x_0 = 0$ and $x_{k+1} = 1$. Then, for every $i = 1, \dots, k$, set

$$x_i = q_i + \tilde{A}(q_i) - 1.$$

The grid obtained in the last algorithm can be reused throughout the estimation process, at every gradient descent step and with every different set of values for the parameter vector θ . With this grid and with a parameter vector θ we can now build a lightweight version of h_{θ} that can be used to evaluate the penalized log-likelihood. Early experiments also suggest that selecting spline knots for p_{θ} according to Algorithm 1 is key to the construction of an unbiased estimator A_{θ} .

Algorithm 2. Let W_{θ} be a semiparametric Williamson transform. To build an approximation for h_{θ} , follow these steps:

1. Set $t_0 = 0$ and $t_{k+1} = 1$. Then, for every $i = 1, \dots, k$, set $t_i = t_{\theta}(x_i)$.
2. For every $i = 1, \dots, k$, set $A_i = \frac{1}{2}(1 + x_i + W_{\theta}(x_i))$.
3. For every $i = 1, \dots, k$, set

$$A'_i = \frac{1 + W'_{\theta}(x_i)}{1 - W'_{\theta}(x_i)}.$$

4. For every $i = 1, \dots, k$, set

$$A''_i = \frac{4W''_{\theta}(x_i)}{(1 - W'_{\theta}(x_i))^3}.$$

5. Set $h_0 = h_{k+1} = 0$. Then, for every $i = 1, \dots, k$, set

$$h_i = 1 + (1 - 2t_i)\frac{A'_i}{A_i} + t_i(1 - t_i) \left[\frac{A''_i}{A_i} - \left(\frac{A'_i}{A_i} \right)^2 \right]. \quad (55)$$

6. Build a piecewise linear interpolator \tilde{h} from the set of points $\{(t_i, h_i)\}_{i=0}^{k+1}$.
7. Calculate the exact value $I = \int_0^1 \tilde{h}$ using the trapezoidal rule and the same set of points $\{(t_i, h_i)\}_{i=0}^{k+1}$.
8. Use $\hat{h} = \tilde{h}/I$ as an approximation for h_θ over $[0, 1]$.

Proof. The rationale of the last algorithm is rather clear. Equation (55) mimics (53), where A_θ and its derivatives are evaluated over t_i indirectly through equations (20), (22) and (23), requiring only the x_i 's and W_θ and its derivatives. On the other hand, the reader can easily check that $h_\theta(0) = h_\theta(1) = 0$, considering all the constraints imposed by our method: $A'_\theta(0^+) = -1$, $A'_\theta(1^-) = 1$ and $f_\theta(x) > 0$ for all $x \in [0, 1]$, etc. The case at the 0 endpoint is not so trivial, but nearly so. After simplification, we arrive at

$$h_\theta(0) = 2f_\theta(0) \lim_{x \rightarrow 0^+} \frac{1+x-W_\theta(x)}{x(1-W'_\theta(x))^3}.$$

Repeatedly applying L'Hôpital's rule, we can check that the denominator tends to zero and, eventually, the whole limit also tends to zero. Finally, the step involving the integral ensures $\int_0^1 \tilde{h} = 1$, making a \tilde{h} a true pdf, which was not automatically granted by the linear interpolation strategy. \square

Algorithm 2 is the cornerstone of the estimation process, as it reduces the gap between W_θ and $\ell(\theta|\mathcal{D})$, dealing with key problems like the approximation of h_θ and the rotation of W_θ . The rest of the estimation procedure is comparatively simpler, but nonetheless we still need to build W_θ .

We start off by building f_θ from the zero-integral spline p_θ using (37). In order not to stop backpropagation, we propose to approximate the integral $\int_0^1 \exp p_\theta$ in the denominator of (37) using the trapezoidal rule. Then, we propose to compute W_θ and its derivatives directly from equations (30), (31) and (32). W''_θ can be easily computed from f_θ . Then, W'_θ and \hat{F}_θ are integral functions that need to be approximated using the trapezoidal rule over a sufficiently fine grid. Finally, W_θ builds upon W'_θ and \hat{F}_θ .

The use of the trapezoidal rule, which speeds up computations and allows backpropagation, may produce inaccurate results on extreme cases, for instance, if the pdf f_θ turns out to be very spiky near 0.⁶ In general, $\int_0^1 p_\theta \approx 1$ is no obstacle for convergence, producing good results. However, if severe deviations occur, the resulting W_θ might violate the constraint $W_\theta(0) = 1$, which in turn would yield a Pickands functions greater than 1. For those *rare* cases, we have devised a very effective mechanism in normalizing the W function so as to secure $W(0) = 1$. This can easily be achieved by dividing the original W by its value $W(0) \neq 1$. The simulation study conducted in Section 4.2 tested the limits of our method at this respect, but the proposed fix considerably improved the results, reducing the appearance of such outlier effects. Other than those extreme cases, we expect the non-normalized procedure to perform well.

⁶A very strong association would be expected in such cases, as expressed by (52).

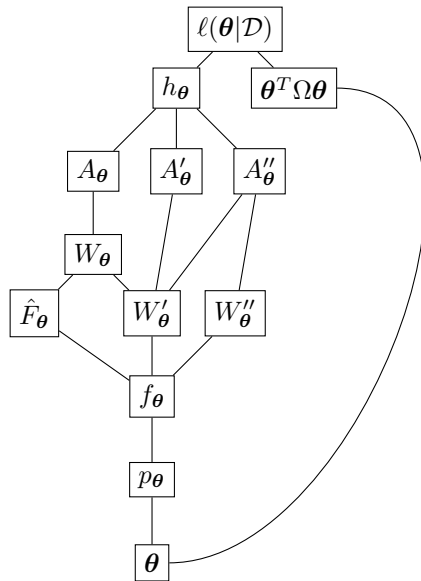


Figure 10: Computation graph for the estimation process, from the bottom parameter vector θ all the way up to the penalized log-likelihood $\ell(\theta|\mathcal{D})$.

3.4.1 Implementation tips

From an implementation perspective, memoization, that is, caching function evaluations, plays a major role in the acceleration of the above estimations. Consider that both W'_θ and \hat{F}_θ include f_θ in their integrands, while W''_θ directly uses it. Then, W_θ uses values from W'_θ and \hat{F}_θ , the former of which is also used on its own by Algorithm 2. Also, note that Algorithm 2 only requires the evaluation of W_θ and its derivatives at the x_i 's. Therefore, along memoization, the trapezoidal rules for approximating W'_θ and \hat{F}_θ may benefit from using the same x_i 's as a discrete integration domain.

Figure 10 shows the full computation graph of the estimation process. Interestingly, gradients can be computed from the top penalized log-likelihood all the way down the parameter vector using backpropagation. For that matter, we recommend using the `autograd` package [38], capable of performing automatic differentiation on native Python operations.

In order to adapt the estimation process to the particular hypotheses of our method, we propose to change the copula variable ordering whenever a steep slope is likely to appear for W_θ near 0, which coincides with the minimum of A_θ being placed at $t < 0.5$. This situation can heuristically be assessed by calculating the mode of the pdf h , as suggested in [19]. If the mode is placed at $t < 0.5$, then the minimum of the Pickands function is *likely* to be placed at $t < 0.5$. We support the hypothesis of [19] based on our own experience. Therefore, whenever the mode is placed at $t < 0.5$, we recommend changing the variable ordering before estimating and then flip the resulting Pickands function A as $\hat{A}(t) = A(1 - t)$.

3.5 Simulation

Once the parameters θ have been estimated, we propose to subsequently estimate W_θ and A_θ . From that point on, querying the model (simulating, estimating probabilities, etc.) will be equivalent to evaluating the Pickands function A_θ , as with any other EVC.

Both W_θ and A_θ are convex functions. Therefore, to achieve enough accuracy we recommend to approximate not only the function values, but also those of their derivatives up to second order. In both cases, we recommend to build fine-grained spline $\mathcal{C}^2([0, 1])$ approximations \widetilde{W} and \widetilde{A} over $[0, 1]$. Notice, however, that some derivatives may take non-finite values. In what follows, we shall assume that non-finite values are to be ignored in the interpolation process, imposing no constraint.

The estimation of W_θ requires approximating two integral functions that have no closed form, in general. Its second derivative, though, can be straightly computed from p_θ .

Algorithm 3. Let p_θ be the resulting zero-integral spline (45) from the estimation process and let $\{x_i\}_{i=0}^{m+1}$ be an interpolation grid such that $0 = x_0 < x_1 < \dots < x_{m+1} = 1$. To build an approximation to the corresponding Williamson transform W_θ , follow these steps:

1. Compute an approximation $I \approx \int_0^1 \exp p_\theta$.
2. Define the approximation $\tilde{f}(x) = \frac{\exp p_\theta(x)}{I}$.
3. Set $W_0'' = \infty$. Then, for every $j = 1, \dots, m+1$, set $W_j'' = \frac{1}{I} \frac{\tilde{f}(x_j)}{x_j}$.
4. For every $j = 1, \dots, m$, compute the approximations

$$P_j \approx \int_{x_j}^{x_{j+1}} \tilde{f}(r) dr, \quad S_j \approx \int_{x_j}^{x_{j+1}} \frac{\tilde{f}(r)}{r} dr.$$

5. Set $W_{m+1}' = 0$ and $W_0' = -\infty$. Then, for every j from m down to 1 , compute W_j' using the recurrence relation

$$W_j' = W_{j+1}' - S_j. \quad (56)$$

6. Set $W_{m+1} = 0$ and $W_0 = 1$. Then, for every j from m down to 1 , compute W_j using the recurrence relation

$$W_j = W_{j+1} + x_j W_j' - x_{j+1} W_{j+1}' + P_j. \quad (57)$$

7. Build a spline interpolator \widetilde{W} such that $\widetilde{W}(x_j) = W_j$, $\widetilde{W}'(x_j) = W_j'$ and $\widetilde{W}''(x_j) = W_j''$, for every $j = 0, \dots, m+1$.
8. Use \widetilde{W} as an approximation for W_θ over $[0, 1]$.

Proof. The rationale of this algorithm consists in the approximation of W_θ by a spline that takes into account up to second derivatives. Clearly, W_j'' is a straight approximation for $W_\theta''(x_j)$, thus it only remains to check that (57) and (56) provide good approximations for $W_\theta(x_j)$ and $W_\theta'(x_j)$, respectively.

First, note that

$$W_j' = \sum_{k=j}^m W_k' - W_{k+1}' = - \sum_{k=j}^m S_j \approx \int_{x_j}^1 \frac{f_\theta(r)}{r} dr. \quad (58)$$

Similarly,

$$\begin{aligned} W_j &= \sum_{k=j}^m W_k - W_{k+1} = \sum_{k=j}^m x_k W_k' - x_{k+1} W_{k+1}' + P_k \\ &= x_j W_j' + \sum_{k=j}^m P_k \\ &\approx x_j W_\theta'(x_j) + \int_{x_j}^1 f_\theta(r) dr \end{aligned} \quad (59)$$

and the right-hand side equals $W_\theta(x_j)$, using (32). \square

The recurrent schemes (57) and (56) preserve the 2-monotonicity property of the underlying W_θ . Indeed, unfolding (56), we have $W_1' \leq W_2' \leq \dots \leq W_{m+1}' \leq 0$. On the other hand, plugging (56) into (57), we get

$$W_j - W_{j+1} = -(x_{j+1} - x_j) W_{j+1}' + P_j - x_j S_j \geq 0,$$

since $W_{j+1}' \leq 0$ and $P_j \geq x_j S_j$. Also, note that $W(x_1) < 1$.

Altogether, the computation of the derivatives contained in both recurrences allow to form a dataset of graph dots that is compatible with the shape of a Williamson transform. Points $\{(x_j, W_j, W_j')\}_{j=1}^{m+1}$ could be input to the shape-preserving [47] interpolation procedure by Schumaker, which would guarantee that the resulting quadratic spline is 2-monotone over the whole domain. However, in general, the second derivative of such a spline would not be continuous, which would hinder the simulation process, since the density of an EVC is connected to W'' . In practice, for the intended use of this approximation, shape preservation is not mandatory and smoothness and general accuracy are preferred.

Once estimated W_θ , we proceed to estimate A_θ .

Algorithm 4. Let \widetilde{W} be the estimate obtained through Algorithm 3 and let $\{t_i\}_{i=0}^{m+1}$ be an interpolation grid such that $0 = t_0 < t_1 < \dots < t_{m+1} = 1$. To retrieve the Pickands function A_θ , follow these steps:

1. Set $x_0 = 0$ and $x_{m+1} = 1$. Then, for every $i = 1, \dots, m$, find the $x_i \in (0, 1)$ such that $t(x_i) = t_i$, using \widetilde{W} in (20).
2. Set $A_0 = A_{m+1} = 1$. Then, for every $i = 1, \dots, m$, take $A_i = A(t(x_i))$, using \widetilde{W} in (20).
3. Set $A'_0 = -1$ and $A'_{m+1} = 1$. Then, for every $i = 1, \dots, m$, take $A'_i = A'(t(x_i))$, using \widetilde{W}' in (22).

4. Set $A_0'' = \infty$ and $A_{m+1}'' = 4\widetilde{W}''(1)$. Then, for every $i = 1, \dots, m$, take $A_i'' = A''(t(x_i))$, using \widetilde{W}'' in (23).
5. Build a spline interpolator \widetilde{A} such that $\widetilde{A}(t_i) = A_i$, $\widetilde{A}'(t_i) = A_i'$ and $\widetilde{A}''(t_i) = A_i''$, for every $i = 0, \dots, m+1$.
6. Use \widetilde{A} as an approximation for A_θ over $[0, 1]$.

Using A_θ we can evaluate C_θ and its partial derivatives, which are the only requirements for the oldest and simplest general copula simulation algorithms [7]. The following is also the most convenient method in a bivariate setting.

Algorithm 5. Let \widetilde{A} be the approximation to A_θ obtained through Algorithm 4 and \widetilde{C} its corresponding EVC, approximating C_θ . To draw a sample $\{(U_i, V_i)\}_{i=1}^n$ from $(U, V) \sim C_\theta$, follow these steps:

1. For every $i = 1, 2, \dots, n$, draw $U_i \sim \text{Unif}[0, 1]$, $U_i > 0$.
2. For every $i = 1, 2, \dots, n$, draw $P_i \sim \text{Unif}[0, 1]$, $P_i > 0$.
3. For every $i = 1, 2, \dots, n$, set V_i as any solution in $(0, 1)$ to

$$\frac{\partial \widetilde{C}}{\partial u}(U_i, V_i) \equiv \frac{\widetilde{C}(U_i, V_i)}{U_i} (\widetilde{A}(T_i) + (1 - T_i)\widetilde{A}'(T_i)) = P_i, \quad (60)$$

where $T_i = \log(U_i)/\log(U_i V_i)$.

This algorithm simulates the second component V_i of the bivariate vector by simulating the P_i -quantile of the conditional distribution $[V|U = U_i]$, given by the partial derivative of $\partial C_\theta/\partial u$, according to (7). In general, the solution to (60) is not unique. Nevertheless, whenever a whole solution interval $(a, b]$ exists, we would have $\mathbb{P}(a < V \leq b | U = U_i) = 0$, meaning all values are equally unlikely and odds are very high against this happening. In practice, the root-finding algorithm [3] proves to be extremely effective. Also, the compact convergence of partial derivatives implied by our method, according to Corollary 2, contributes to the stability of the simulation process.

3.6 Refinement

One of the limitations implied by our method is the fact that an estimated Pickands function A always satisfies $A'(0^+) = -1$ and $A'(1^-) = 1$. This is a direct consequence of our construction, which imposes $W'(0^+) = -\infty$ and $W'(1^-) = 0$ on the Williamson transform. In practice, however, these boundary constraints do not hinder the overall expressiveness of the resulting model. Remember that, for instance, upper tail dependence is not linked to either boundary derivative of the Pickands function, but to the mid-point value $A(1/2)$. This contrasts with the nature of another semiparametric procedure like [31], where a slope value completely determined the tail index.

In our method, misspecified slopes for the Pickands function have a much lower impact on the concordance (Blomqvist's beta) and upper tail dependence. Nonetheless, since it might produce a slight bias, we propose a refinement step that could follow our method.

Khoudraji’s method [34] is best known for inducing asymmetry in symmetrical EVCs. However, there is no reason why it should not be used on asymmetrical ones: the input copula being symmetrical is just a special case [44]. Consider a Pickands function A obtained through our method. Differentiating (14) we arrive at

$$\begin{aligned} A'_{\alpha,\beta}(0^+) &= \beta A'(0^+) = -\beta \\ A'_{\alpha,\beta}(1^-) &= \alpha A'(1^-) = \alpha \end{aligned} \quad , \quad (61)$$

where, remember, $\alpha, \beta \in (0, 1]$, retrieving A for $\alpha = \beta = 1$. Even though A is, in general, asymmetrical, we see from (61) that Khoudraji’s method serves our purpose of freely parameterizing the boundary slopes.⁷

It is our belief that adding two more parameters through Khoudraji’s method may improve the fitness of the resulting model in some particular cases, especially for weak correlations. However, the inclusion of the new parameters in the gradient-based optimization seems unworkable, as it would invalidate the interpolation grid in Algorithm 2. A derivative-free optimization involving both the spline parameter vector $\boldsymbol{\theta}$ and the asymmetry parameters α and β could be run, starting from $\alpha = \beta = 1$ and some initial guess $\boldsymbol{\theta} = \boldsymbol{\theta}_0$ obtained through a gradient-based method. In any case, the practical demonstration of such a procedure, beyond its theoretical statement, is out of the scope of this paper.

4 Simulation study

We conducted a simulation study to test the effectiveness of our method on a wide spectrum of cases with high confidence. The simulation study consists of two independent experiments. The first one addresses the bias and variance tradeoffs by repeating the estimation process for a large number of different random samples drawn from a fixed copula. On the other hand, the second experiment aims to cover an even larger array of extreme-value copulas, but fitting a single random sample for each one and emphasizing total variation assessment.

4.1 Bias and variance

The first part of the study consisted of 30 individual experiments, each of them centered on a particular instance of a copula family. For each copula instance, we performed an estimation run with our method on each of a set of 100 different random samples from the copula, for a combined total of 3,000 runs. Then, for each 100-sample experiment, we collected the pointwise means and pointwise 98% confidence intervals of the estimated Pickands functions and compared both functional statistics with the original Pickands function.

For this simulation study we employed two of the families presented in Table 1: the Gumbel family and the Galambos family. These are probably two of the most well-known EVCs. Genest and Nešlehová even studied and found a relation between the two in [24], knowing the similarity of their Pickands functions. In each copula family, we tested up to 5 different values of the unique parameter θ , giving rise to different correlations. Finally, apart from the pure

⁷By convexity, the only EVC with either boundary slope equal to zero is the independence copula, with $A(t) = 1$ for all $t \in [0, 1]$. Therefore, except for this limiting case, both slopes are allowed to vary freely.

form of each Gumbel or Galambos copula, we introduced asymmetry by means of Khoudraji’s device, taking either α or β equal to 0.5 and leaving the other as 1. This configuration was precisely the one that demonstrated higher asymmetry in [23]. As a side note, we remind that the asymmetrical extensions of the Gumbel and Galambos families are known as the Tawn and Joe families, respectively.

Each of the copula random samples was generated with 1,000 observations. Our models were fit using 13 parameters in all cases: 10 more parameters than the ground truth copula families. For the Gumbel copulas, we used a curvature penalty factor $\lambda = 10^{-5}$, whereas for the Galambos copulas we used $\lambda = 10^{-4}$.

The results of the experiments can be assessed in Figure 11, for the Gumbel copulas, and Figure 12, for the Galambos copulas. The results are qualitatively very similar in both cases. Our method displays low biases and variances in all the experiments, with perhaps the only exception of the lowest correlated Gumbel sample, with a slight bias. This behaviour matches the known limitation of our method as regards the boundary slopes, which have fixed values. Therefore, our method is likely to perform a bit worse as variables tend to be more independent. Additionally, according to [33], a wider range of Pickands functions exist for lower correlations, which poses greater difficulties for the optimization process. On the other hand, our method shows high sensitivity when capturing asymmetry, performing well in all cases, especially considering that the limitation of the fixed slopes becomes more apparent in these cases, as shown by (61).

In all simulations we employed the trick mentioned in Section 3.4 for selecting the *a priori* more convenient variable ordering, so as to avoid numerical instabilities. The procedure worked well, as demonstrated by the practically equal results obtained for either $\alpha = 0.5$ or $\beta = 0.5$. Note that otherwise we could have run the optimization for both variable orderings, taking the one with the highest fitness, but at a higher execution time.

4.2 Total variation

In the second part of the simulation study we generated $n = 200$ random extreme-value copulas by utilizing our own construction method.

First of all, we chose the affine spline model (46) as the first building block, assuming uniformly distributed knots and a total of $d = 13$ parameters. Let us call $\boldsymbol{\theta}_0 \in \mathbb{R}^d$ the coordinates of the center of the affine model. We then ran an MCMC simulation assuming the model coordinates $\boldsymbol{\theta}$ in (44) were distributed according to the following pdf:

$$p(\boldsymbol{\theta}) \propto \begin{cases} e^{-\lambda \bar{\boldsymbol{\theta}}^T \Omega \bar{\boldsymbol{\theta}}}, & \text{if } \|\boldsymbol{\theta}\|_2 \leq R \\ 0, & \text{if } \|\boldsymbol{\theta}\|_2 > R \end{cases}, \text{ for } \bar{\boldsymbol{\theta}} = \boldsymbol{\theta} + \boldsymbol{\theta}_0,$$

where Ω is the curvature matrix of the underlying spline, as described in Section 3.4, and λ and R are free hyper-parameters. The previous model is the truncated version of an improper prior based on curvature penalization, with factor λ . The support of the distribution is the hyperball of radius R .

We tuned the hyper-parameters with values $\lambda = 10^{-4}$ and $R = 5$ so that the resulting splines covered a wide range of correlations (in the sense of the Gini coefficient (50)) and were at the same time smooth. Finally, in order to prevent

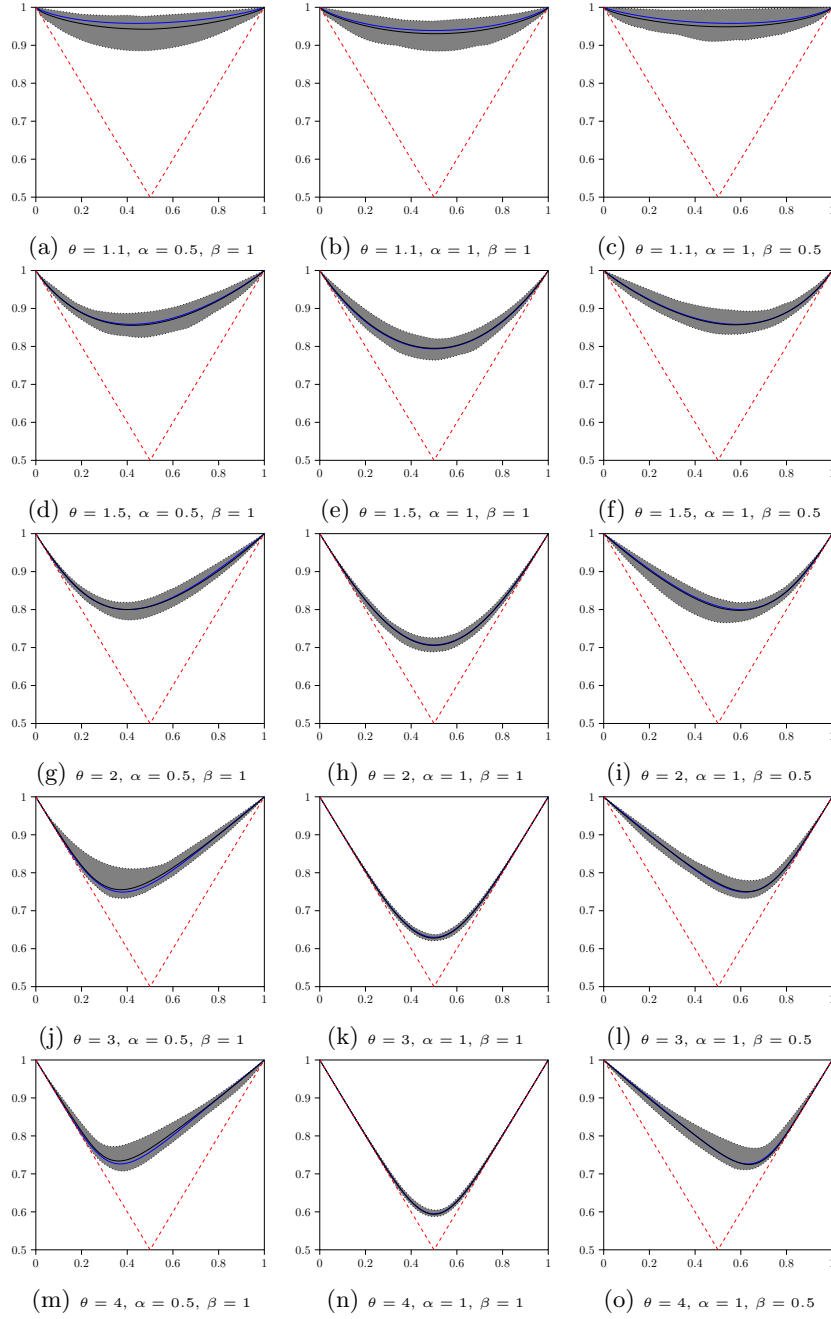


Figure 11: Simulation study for the Gumbel family. The blue line designates the ground-truth Pickands function, whereas the black one corresponds to the pointwise mean of the estimations. The shaded areas represent 98% pointwise confidence intervals for the estimates.

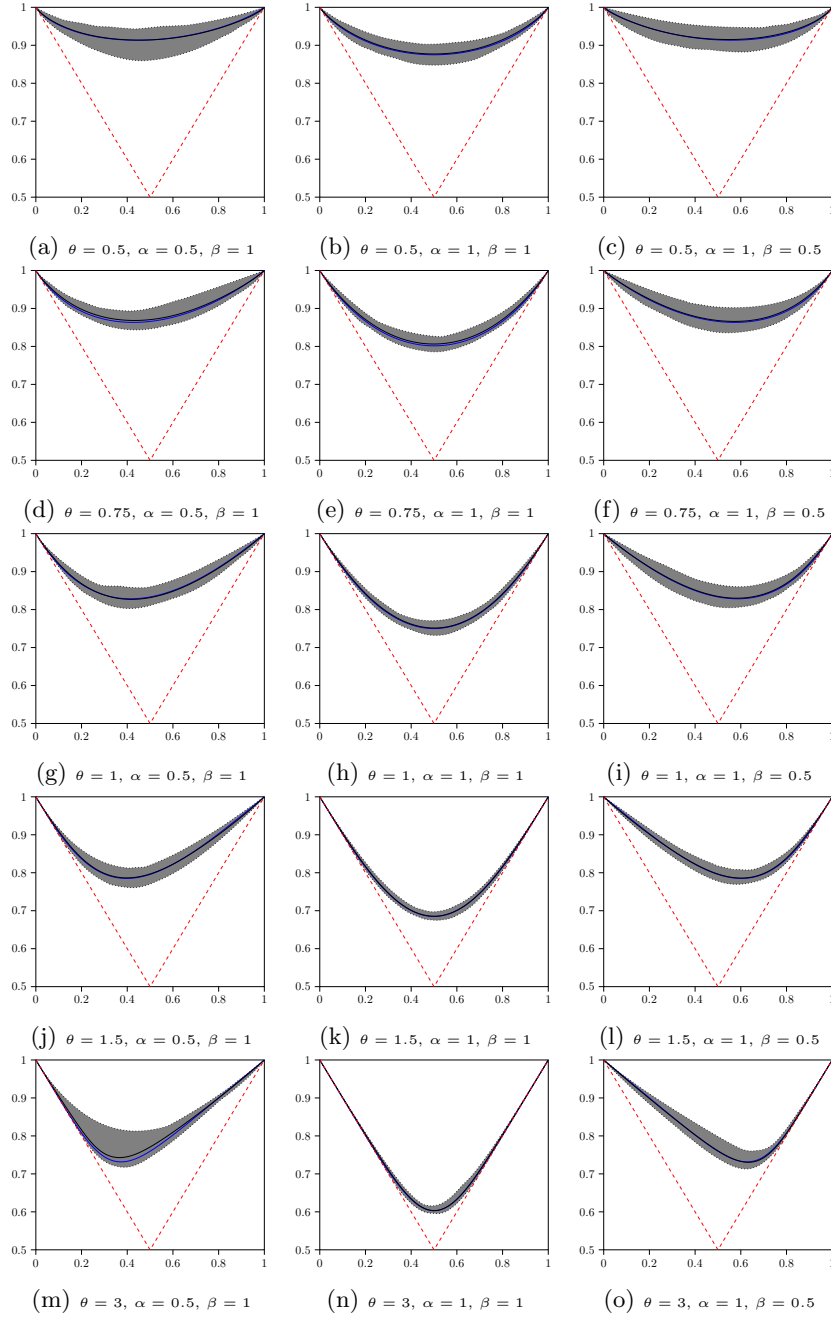


Figure 12: Simulation study for the Galambos family. The blue line designates the ground-truth Pickands function, whereas the black one corresponds to the pointwise mean of the estimations. The shaded areas represent 98% pointwise confidence intervals for the estimates.

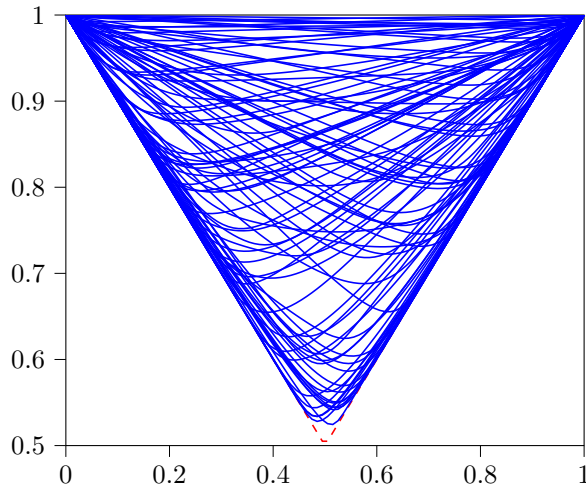


Figure 13: A subsample of size 100 from the whole population of random Pickands functions used in the second part of the simulation study.

any kind of asymmetry, we replaced the even elements in the sequence by its corresponding mirrored versions $\tilde{A}(t) = A(1 - t)$. Figure 13 shows a subsample of the generated random Pickands functions. The area between the support lines and the upper bound line is covered in a fairly balanced way. In this part of the simulation study we also employed the heuristic to determine the most suitable variable ordering, and thus we expected our method to perform well regardless of the orientation of the Pickands function.

For each element in the sequence $\{\theta_i\}_{i=1}^n$, we built the EVC C_{θ_i} and performed several estimation runs on random samples of different sizes $\{S_j\}_{j=1}^m$. All fitted models had the same number of parameters as the ground truth splines ($d = 13$) and also employed the same affine translation. The penalty factor in the loss function (54) was also set to $\lambda = 10^{-4}$. The only aspect in which estimated models differed from ground truth is spline knot placement, which was uniform for the latter, but empirically assessed for the former. Then, for each sample size S_j , we estimated a copula C_{ij} using our method and assessed divergence from ground truth by means of total variation distance

$$d_{\text{TV}}(C_{\theta_i}, C_{ij}) = \frac{1}{2} \int_{[0,1]^2} |c_{\theta_i}(u, v) - c_{ij}(u, v)| \, dudv, \quad (62)$$

where c_{θ_i} and c_{ij} are the pdfs of C_{θ_i} and C_{ij} , respectively. The total variation defined in (62) is the bivariate counterpart of Definition 2 and thus provides an upper bound on the difference between the measured values of each copula on any measurable set $B \subset [0, 1]^2$. Therefore, (62) is a very conservative evaluation measure.

The main summary statistics from the experiment are presented in Table 2. The table shows reasonable mean and quantile values for total variation, considering the intrinsic complexity of the ground truth models and the finiteness of sample sizes. Mean values are below 0.10 regardless of sample size and the 50% and 75% quantiles are even more promising, being generally below 0.05 and 0.07, respectively. Interestingly, Table 2 shows that total variation decreases, in

	mean	10%	25%	50%	75%	90%
sample size						
250	.09754	.02172	.03447	.04927	.07999	.13676
500	.08693	.01543	.02832	.04385	.06958	.13223
1000	.08137	.01606	.02461	.03544	.06803	.13237
2000	.06946	.01238	.02067	.0314	.05429	.10773

Table 2: Main summary statistics from the experiment, mean and quantiles, for each sample size. Total variation decreases as sample size increases.

general, as the sample size increases. Figure 14 and Figure 15 show the existence of some outliers, with abnormally high values of total variation, that are responsible for the mean and the median being so far from each other.

We collected the value of the Gini coefficient for each random copula in order to better assess the nature of those outliers. It turns out that all of them correspond to extremely high values of the Gini coefficient (above 98%), which could be geometrically interpreted as the Pickands function lying very close to the support lines. This is demonstrated by the regression tree depicted in Figure 16. High values of the Gini coefficient test the hypotheses of our method and hinder the estimation process. No matter how many spline knots and parameters are used, there will always be sufficiently highly correlated copulas that will put stress on our method. Notwithstanding, the normalization procedure on the W function mentioned in Section 3.4 helps to mitigate such effects.

5 Real data applications

We will next present some results of our method on non-simulated data.

5.1 Context

In the year 2015, the LIGO⁸ Scientific Collaboration and the Virgo Collaboration announced the first direct detection of a gravitational wave, produced by the merger of a binary black hole [1]. The existence of gravitational waves, ripples in the fabric of space-time, was predicted by Einstein’s theory of general relativity in 1916 [9] as a mathematical construct that many thought at that time to have no physical meaning. It took nearly a century from its prediction and 60 years of search to experimentally ascertain the discovery, opening a new era for astronomy.

Only the most extreme events in the Universe (supernovas, massive body mergers, Big Bang primordial fluctuations, etc.), in terms of energy, are able to generate gravitational waves strong enough to be detected by current experimental procedures, due to the small value of the gravitational constant [9], which expresses the rigidity of space-time. A significant amount of human and material resources is needed to detect gravitational waves. Specifically, sufficiently sensitive interferometers need to have arms several kilometers long. Additionally, in order to discriminate between true detections and spurious local

⁸Laser Interferometer Gravitational-Wave Observatory.

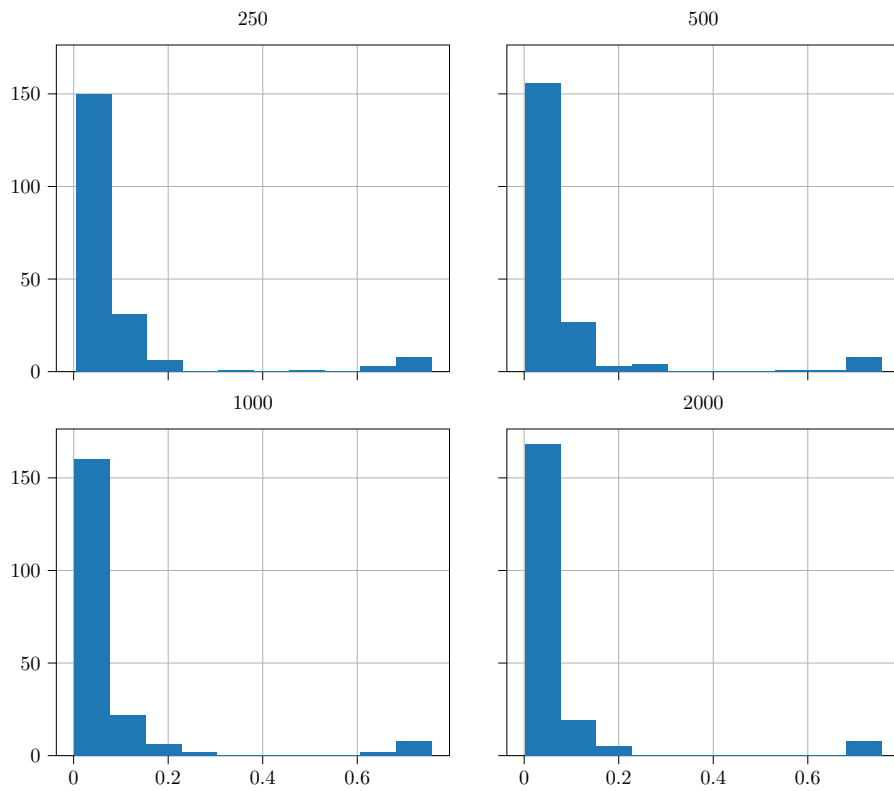


Figure 14: Histograms of the total variation distributions for each sample size.

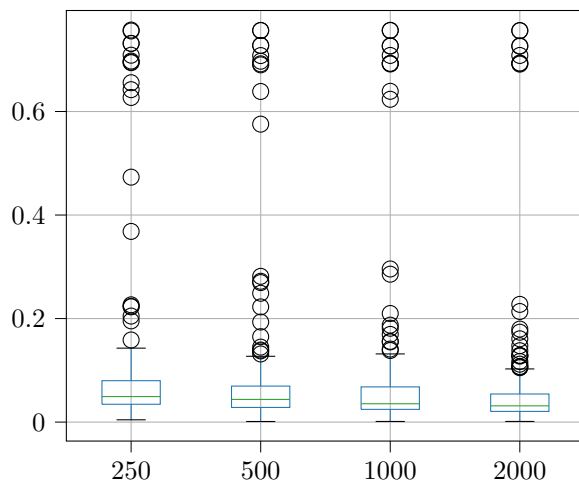


Figure 15: Box plots of the total variation distributions for each sample size.

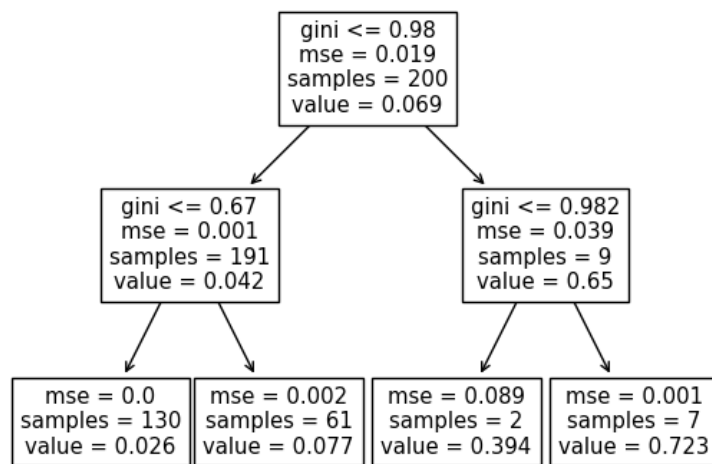


Figure 16: Regression tree (depth 2) of total variation on the Gini coefficient. Issues were encountered on a few (9 out of 200) cases in which the Gini coefficient was above 98%.

signals (electromagnetic radiation, earthquakes, etc.), several detectors, highly separated from each other, are needed.

LIGO, settled in the United States, with two laboratories, was the first detector of a global advanced network that aims to increase accuracy and exhaustiveness of discoveries [1], soon to be joined by others, most notably Virgo, in Italy. Despite LIGO and Virgo joining efforts, the first detection was only reported by LIGO, since the Virgo facilities were not operating at that time for upgrading reasons. Since the first detection in 2015, a total of 50 events have been confirmed by the joint collaboration of LIGO and Virgo. All of them correspond to massive body mergers, mainly black holes and neutron stars.

5.2 Data

We have chosen the gravitational wave detection dataset gathered by the LIGO and Virgo collaborations during their first three observation runs to test the applicability of our method. It consists of 50 rows and two columns. Each row represents a merger event, while each column features one of the masses involved in the event, measured in solar mass units (M_{\odot}). During the first and second observation runs, 11 events were detected, while the third run provided 39. The first event was GW150914, on september 2015, and the last one, GW190930_133541, on September 2019. As presented by LIGO and Virgo, the first mass is always the larger of the two and is known as the primary mass, whereas the other one is named the secondary mass.

We reckon that very few datasets are more representative of bivariate data, considering the very nature of binary mergers. Bivariate models are usually building blocks for higher dimensional ones, but in this case all the attention is centered around two mass values, of high scientific relevance. Another aspect that adds up to this significance is the scarcity of data, for only 50 events have been recorded during a 5-year span. This contrasts with the increasingly huge amounts of information coming from IoT, social networks, finance, etc., in the current era of Big Data.

5.3 Disclaimer

The purpose of this section is to test our method on real world data. Our results shall not be considered by any means of any relevance for the physics research community. On this paper we have not counted on any expert in physics to assess the relevance of our results. Much on the contrary, we have preferred to see data from an amateur perspective, as one of our method goals is exploratory data analysis. To gain a deeper understanding of the physical phenomena, professional researchers make use of parametric models grounded on a solid theoretical base [2]. On the other hand, a semiparametric technique like ours provides a reasonable compromise between robustness and speed of prototyping.

5.4 Statistical model

As mentioned above, the dataset consists of 50 bivariate observations $\mathcal{D} = \{(M_1^{(i)}, M_2^{(i)})\}_{i=1}^{50}$, where $M_1^{(i)} \geq M_2^{(i)}$. The last censoring constraint makes the

dataset not directly tractable by our method, best suited for copulas supported on the whole $[0, 1]^2$, unless conveniently preprocessed.

LIGO and Virgo perform a statistical analysis of the joint mass distribution in [2]. To do so, they consider two separate univariate models. The first one, models the primary mass M_1 unchanged, whereas the second one models the *mass ratio* $Q = M_2/M_1$ conditioning on M_1 . Since $M_1 \geq M_2$, by definition, the resulting model captures by construction the censoring constraint. The final joint model is formed by the vector (M_1, QM_1) .

On this paper we will take a different approach. Instead of considering a ratio variable to be later multiplied by the primary mass to calculate the secondary mass, we will directly tackle the modelling of a bivariate mass vector. To be able to apply our method, we turned the censoring problem into an exchangeable one, where both masses played the same role. Of course, the original dataset \mathcal{D} does not allow such a treatment, so we had to hypothesize a new sample space where primary masses are detected with 50% probability at the first vector component and with 50% at the second one. Such a scenario would occur if detections of an event reported masses indistinctly of their relative order.

Regardless of its physical significance, considering both masses indistinctly would allow us to fit a single univariate model shared by both masses, which, in turn, would help to focus on the main purpose of our experiment, the bivariate dependency, reducing the overall model complexity. Besides, it would be an illustrative experience to capture in a single stellar mass model as many data points as possible. Later on we would find out that a bivariate mass model was indeed a much more interesting and tractable problem with the tools of extreme-value copulas at our hands.

To perform such an analysis, we built a new sample $\tilde{\mathcal{D}} = \{(\tilde{M}_1^{(i)}, \tilde{M}_2^{(i)})\}_{i=1}^{100}$, where, for $j = 1, 2$,

$$\tilde{M}_j^{(i)} = \begin{cases} M_j^{(i)}, & \text{if } i \leq 50 \\ M_{1+j \bmod 2}^{(i-50)}, & \text{if } i > 50 \end{cases}.$$

Using the previous up-sampled and symmetrical dataset, we fitted (i) a single univariate mass model f for both margins and (ii) a copula model C of the dependency between mass ranks. Note that with the transformed sample, the number of observations available for model fitting doubled, which could help to overcome the data scarcity.

With these tools we targeted a random vector $(\tilde{M}_1, \tilde{M}_2)$. In order to retrieve the original primary-secondary mass model, we just had to take $M_1 = \max\{\tilde{M}_1, \tilde{M}_2\}$ and $M_2 = \min\{\tilde{M}_1, \tilde{M}_2\}$.

5.4.1 Univariate margin model

For the univariate margin mass model we decided to employ a semiparametric model too, in order to make up for our lack of expertise in relation to stellar mass models. We wanted the data present in the dataset to speak by itself. We first considered using Kernel Density Estimation, but eventually discarded it because of the mass variables being bounded. Then, we successfully tried out the very same technique we used for modelling the density f in (29): Bayes space densities built from ZB-splines.

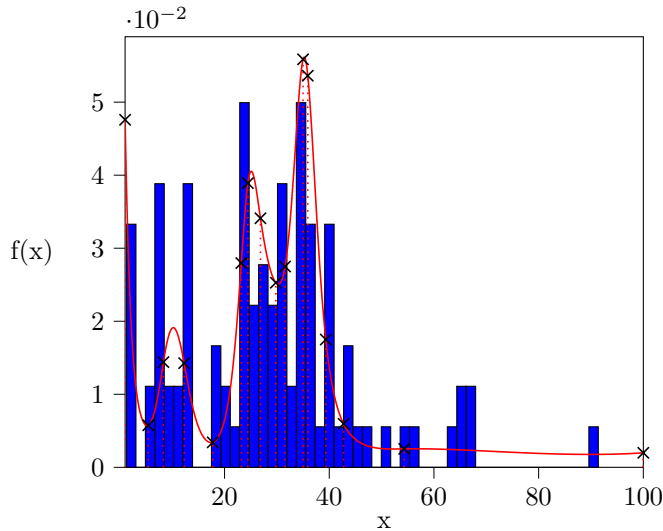


Figure 17: Univariate margin mass model pdf, fitted using ZB-splines back-transformed into the Bayes space. The vertical cuts correspond to the underlying spline knots.

The result of our experiment is shown in Figure 17 and Figure 18. We selected 17 parameters, with knots distributed according to the original sample between $1 M_{\odot}$ and $100 M_{\odot}$, and a curvature penalty factor of 10. The first mode, near $1 M_{\odot}$, mostly corresponds to neutron stars; black hole masses typically range beyond $5 M_{\odot}$.

5.4.2 Bivariate copula model

Letting \hat{F} be the empirical CDF of the univariate sample $\{\tilde{M}_1^{(i)}\}_{i=1}^{100}$ (equivalently, from $\{\tilde{M}_2^{(i)}\}_{i=1}^{100}$), we decided to fit a copula pseudo-sample $\tilde{\mathcal{D}}_{\text{cop}}$, independent of the fitted margin model from the previous section:

$$\tilde{\mathcal{D}}_{\text{cop}} = \{(\tilde{U}_1^{(i)}, \tilde{U}_2^{(i)})\}_{i=1}^{100} = \{(\hat{F}(\tilde{M}_1^{(i)}), \hat{F}(\tilde{M}_2^{(i)}))\}_{i=1}^{100}.$$

The applicability of EVC was readily made clear after inspecting $\tilde{\mathcal{D}}_{\text{cop}}$, where the mirrored data points resembled some characteristic patterns we saw during a random EVC generation phase. Namely, data points were not distributed along the diagonal $\{u = v\}$, but instead described two curved paths that met at both lower and upper tail corners. Correlation was also rather high, which, according to [33], would narrow down the range of admissible Pickands functions, reducing variance.

However, data inspection also revealed absence of upper tail dependence, while lower tail dependence being present. This behaviour did not match the features of EVC. As a matter of fact, it was quite the opposite situation, since EVC, in practice, never have lower tail dependence, but they do have dependence in the upper tail. Luckily, in copula theory we can resort to *survival copulas* whenever a switch between lower and upper tails is needed, as recommended in [19]. If a random vector with uniform margins (U, V) is distributed

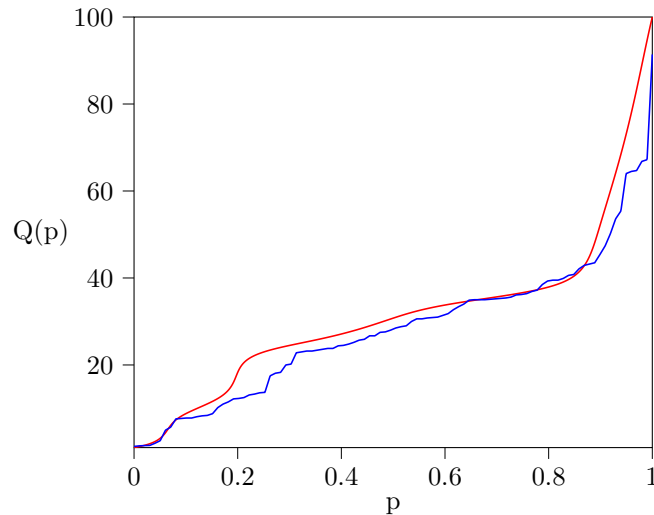


Figure 18: Quantile function of the univariate margin mass model. The blue line corresponds to the empirical quantile, whereas the red one corresponds to the fitted model.

according to a copula C , then $(1 - U, 1 - V)$ follows the survival copula [7, 25]

$$\check{C}(u, v) = u + v - 1 + C(1 - u, 1 - v).$$

The bivariate copula sample $\tilde{\mathcal{D}}_{\text{cop}}$ was accordingly transformed:

$$\tilde{\mathcal{D}}_{\text{surv}} = \{(1 - \tilde{U}_1^{(i)}, 1 - \tilde{U}_2^{(i)})\}_{i=1}^{100}.$$

Of course, once the \check{C} is fitted from sample $\tilde{\mathcal{D}}_{\text{surv}}$, the original copula can be retrieved by taking C equal to the survival copula of \check{C} .

An extreme-value dependence test [26], implemented in the function `evTestK` of the R package `copula`, confirmed our intuition about the applicability of EVC, yielding a p-value higher than 0.35.

The copula model was configured with a cubic (orthonormal) ZB-spline basis with 13 elements, a curvature penalty factor of 10^{-5} and an interpolation grid size of 80 ($k + 2 = 80$ in Algorithm 2) knots.

Figure 19 shows the final state of the internal functions defined in the Williamson transform domain. As we can see, the resulting Bayes density is bimodal, yielding a Williamson transform with an almost linear region. On the other hand, Figure 20 shows the estimated Pickands function and its correspondent h density (53). Despite the sample $\tilde{\mathcal{D}}_{\text{surv}}$ being exchangeable, the h estimate fails to be perfectly symmetrical, with the right peak a bit higher than the one on the left. This was not completely unexpected, given that our method does not address symmetry specifically. Taking that into account, Figure 20 shows that symmetry is reasonably well captured. Notwithstanding, before reversing the survival model, we decided to apply a symmetrization procedure on the resulting Pickands function A , considering $\tilde{A}(t) = [A(t) + A(1 - t)]/2$.

Figure 21 shows the result of the Bayesian posterior distribution of Pickands functions, using the previous MAP estimate as initial guess for the MCMC sampling.

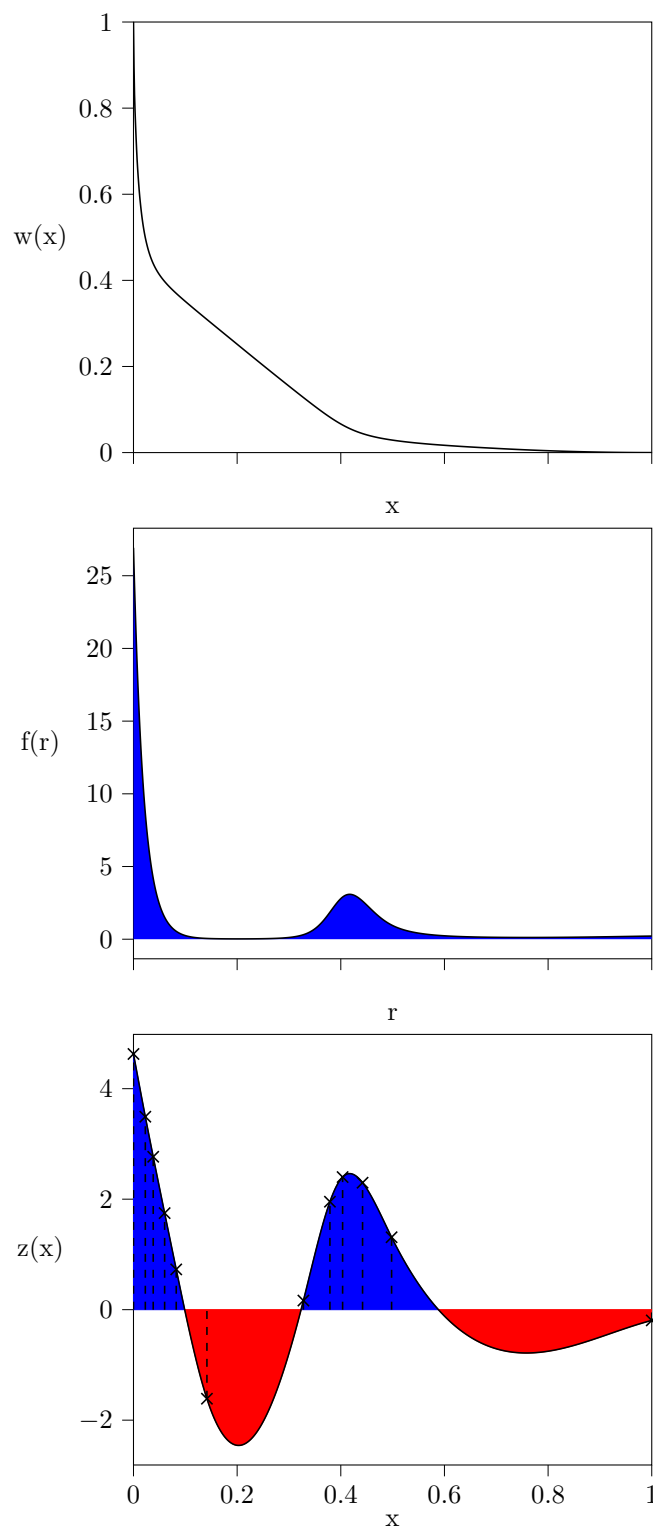


Figure 19: Internal function constructs z (zero-integral spline), f (Bayes density) and W (Williamson transform). The plot displays the underlying spline knots of z .

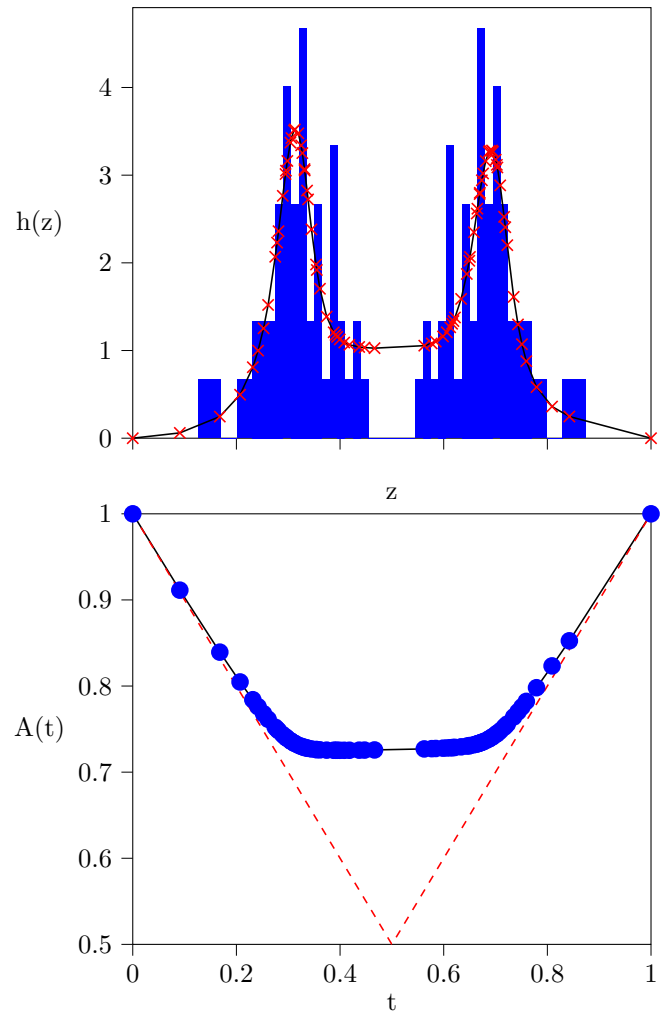


Figure 20: Pickands function A and target density h . The knots represent the function values at the t_i 's grid defined in Algorithm 2.

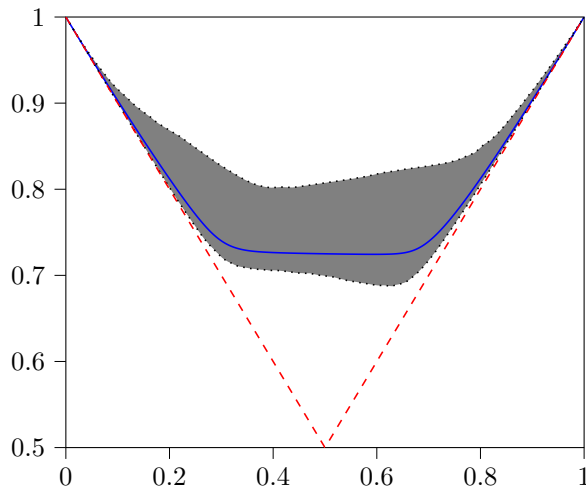


Figure 21: Confidence interval and mean of the posterior Pickands functions sample from a MCMC run.

Finally, Figure 22 shows a sample-density plot of the final copula, after symmetrization and reversal of the survival transformation. The pdf captures the presence of lower tail dependence and the absence of upper tail dependence. Also, there exists a remarkable density gap in the region surrounding the diagonal $\{u = v\}$, which means that binary mergers involving similar masses are rare.

5.4.3 Joint model

Once fitted both the univariate margin mass model (ZB-splines), with pdf f and CDF F , and the copula model (survival symmetrical extreme-value copula), with pdf c , the final joint model immediately followed. Figure 23 shows the joint density of the final model, which is

$$f(x, y) = c(F(x), F(y)) \cdot f(x) \cdot f(y).$$

On the other hand, Figure 24 plots the original LIGO-Virgo dataset against a random sample generated from the previous model, when the first and second components are taken to be the maximum and the minimum, respectively, in order to match the original dataset criterion, as mentioned earlier. There are 10 times more random samples than original data points, for a total of 500. Our model captures three main clusters, concentrated in the regions $[0, 20]^2$, $[20, 40] \times [0, 20]$ and $[20, 40]^2$. It is also worth mentioning there seems to be a barrier at $\{M_2 = 40\}$. Overall, the latter is probably the most controversial prediction of our model, in contrast to the reported models in [2], and a clear sign of *overfitting*: 30 parameters (17 univariate + 13 copula) for only 50 observations (100 after up-sampling).

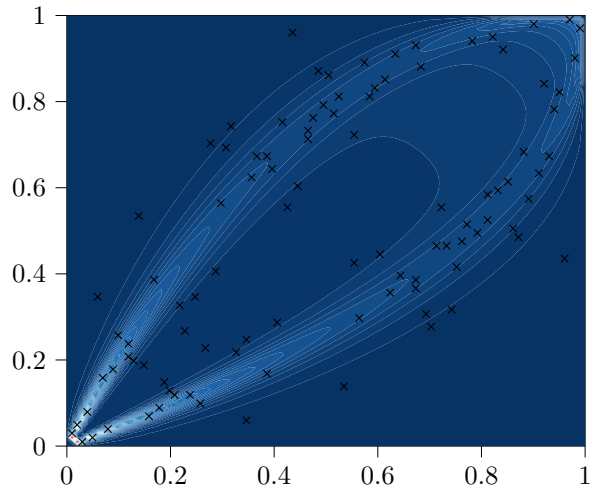


Figure 22: Final copula pdf after symmetrization and reversal of the survival transformation. The data points shown belong to the $\tilde{\mathcal{D}}_{\text{cop}}$ dataset.

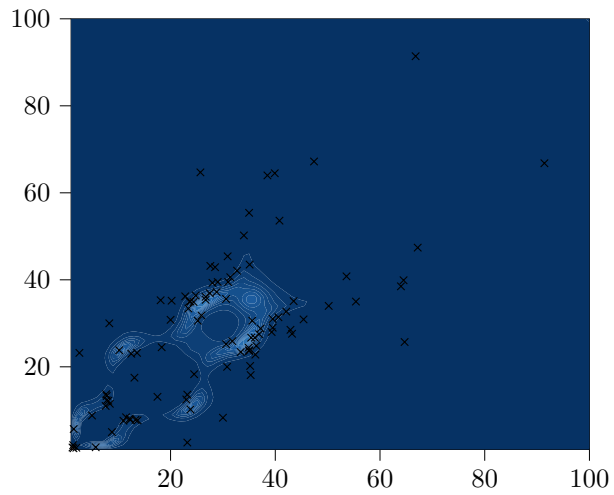


Figure 23: Joint pdf for the final model. The data points shown belong to the $\tilde{\mathcal{D}}$ dataset.

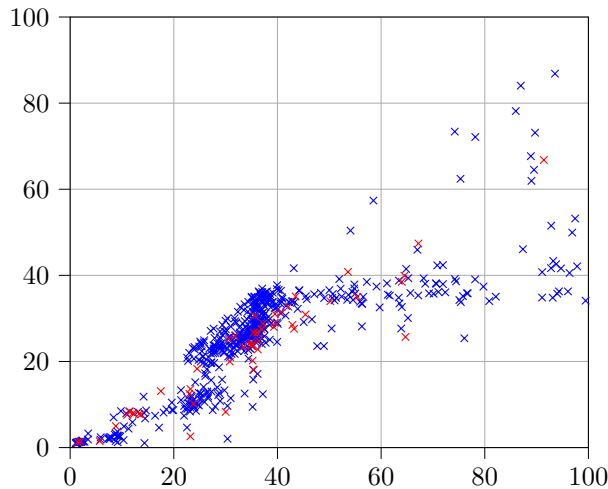


Figure 24: Original masses (red) against random samples from our model (blue).

6 Discussion

In section 3 we introduced a new semiparametric method for extreme-value copula estimation, along with some theoretical and practical results. Namely, EVCs built using our method have interesting convergence and dependence properties that relate to an inner pdf that is at the core of the construction.

In section 4 we presented the results of a thorough simulation study consisting of two independent parts. In the first one, we repeatedly performed estimations on random samples from 30 different extreme-value copulas, with varying degrees of concordance and asymmetry, concluding that our method is effective from a bias-variance tradeoff perspective. The method only struggled slightly on low concordance samples, which could be expected on the theoretical results of [33]. On the other hand, the second part of the simulation study put hard stress on our method, as it was applied on 200 random EVCs and evaluated according to a conservative metric like total variation distance. Our method generally performed very well, providing relatively low total variations with respect to ground truth. Additionally, performance improved as sample sizes increased. The only issue encountered relates to numerical instabilities that hinder the estimation process on rare settings with extremely high correlations.

In section 5 we tested our method on real data from a very especial origin: the LIGO and Virgo binary merger detections. The symmetrical marginally-uniform sample used turned out to be consistent with the extreme-value dependence structure, according to a statistical test. After fitting a flexible univariate model for both margins, we fitted an extreme-value copula for the survival version of the data using our method. The resulting Pickands function had a very peculiar nearly flat shape, due to the bimodality of the underlying fitted sample. Overall, we had the opportunity to graphically assess the high flexibility of the fitted EVC model, which, in conjunction with the univariate margin models, produced a very convincing synthetic dataset for binary mergers.

The main contribution of our work is the proposal of a new semiparametric estimator that allows to fit parameters of an extreme-value copula in a fully

unconstrained manner. This way, our construction allows generating random extreme-value copulas at will, with all the theoretical constraints automatically ensured.⁹ To do so, we rely on basic but powerful transformations, that eliminate step by step all the stringent constraints imposed by the Pickands function. Thanks to this flexible and simple procedure, extreme-value copulas could be studied, for instance, in the context of information geometry as finite-dimensional objects. Finally, we demonstrated the feasibility of our approach, showing that, despite all the operations involved, likelihood-based optimization can be successfully performed with the available software tools and algorithms.

6.1 A quick note on software architecture

Both the simulation study and the LIGO-Virgo application would not have been possible without the large repertoire of software artifacts currently available. We will take a brief moment to mention the most fundamental tools we have used.

First of all, our method, fully implemented in *Python* [50], was containerized using *Docker* [14], which, apart from being ideal for achieving reproducible research, also helped to move our execution environment to the cloud with *Kubernetes* [49].

All the 100 estimations per experiment in the simulation study were parallelized using *Spark* [48]. To prepare the *Spark* setting with *Kubernetes*, two artifacts were of great help: the *Docker image for Apache Spark* [13] and the *Spark Operator* [27].

Finally, *Argo CD* [4] turned out to be really useful to manage all our experiments, to be run on *Kubernetes*, from the same and nice user interface, also allowing to retrieve their specifications by connecting the *Kubernetes* cluster to Git.

7 Future work

The work presented in this paper may be continued in several varied ways. A straight research line could demonstrate the applicability of the combination of zero-integral splines and Williamson’s transform in the context of semiparametric models for bivariate Archimedean copulas [41], as an alternative to [31] or other Laplace transform based methods. Precisely, McNeil and Nešlehová introduced Williamson’s transform to characterize multivariate Archimedean copulas and an extension of these: Liouville copulas [40]. Also related to Archimedean copulas, the very same form introduced in this paper would fit the specific case of Lorenz copulas [21].

Also, our method could be conveniently modified to incorporate deep learning approaches. Instead of zero-integral splines, an over-parameterized multi-layer perceptron could be employed, at the risk of losing identifiability and incurring in overfitting. Alternatively, we could follow a similar approach to [35], where a deep neural network architecture is built to mimic the Laplace transform structure of an Archimedean copula, in the context of extreme-value copulas and over Williamson’s transform, instead.

⁹As demonstrated in the second part of the simulation study.

A third research line could combine the developed semiparametric and deep learning techniques for extreme-value and Archimedean copulas at an attempt to model the more expressive Archimax [10] family, which is a superset of both.

Finally, there are some aspects of our method that would benefit from further research. In particular, the fixed slope values of the resulting Pickands function become a barrier that prevents from achieving a fully flexible semiparametric model. Although we proposed a solution, based on Khoudraji's device, there remain questions on its applicability in practice. Namely, a review of gradient-free optimization methods and its suitability for such a task should be conducted.

References

- [1] B. P. Abbott et al. "Observation of Gravitational Waves from a Binary Black Hole Merger". In: *Physical Review Letters* 116.6 (2016). DOI: 10.1103/physrevlett.116.061102.
- [2] R. Abbott et al. "Population Properties of Compact Objects from the Second LIGO–Virgo Gravitational-Wave Transient Catalog". In: *The Astrophysical Journal Letters* 913.1 (May 2021), p. L7. DOI: 10.3847/2041-8213/abe949.
- [3] G. E. Alefeld, F. A. Potra, and Yixun Shi. "Algorithm 748: enclosing zeros of continuous functions". In: *ACM Transactions on Mathematical Software* 21.3 (Sept. 1995), pp. 327–344. DOI: 10.1145/210089.210111.
- [4] Argo Project. *Argo CD. Declarative continuous deployment for Kubernetes*. URL: <https://argoproj.github.io/argo-cd/> (visited on 09/11/2021).
- [5] Tomáš Bacigál. "On Some Applications of Williamson's Transform in Copula Theory". In: *Advances in Intelligent Systems and Computing*. Springer International Publishing, May 2017, pp. 21–30. DOI: 10.1007/978-3-319-59306-7_3.
- [6] Carl de Boor. "Spline Basics". In: *Handbook of Computer Aided Geometric Design*. Elsevier, 2002, pp. 141–163. DOI: 10.1016/b978-044451104-1/50007-1.
- [7] Eric Bouyé et al. "Copulas for Finance - A Reading Guide and Some Applications". In: *SSRN Electronic Journal* (2000). DOI: 10.2139/ssrn.1032533.
- [8] P. Capéraà, A. L. Fougères, and C. Genest. "A nonparametric estimation procedure for bivariate extreme value copulas". In: *Biometrika* 84.3 (Sept. 1997), pp. 567–577. DOI: 10.1093/biomet/84.3.567.
- [9] Jorge Cervantes-Cota, Salvador Galindo-Uribarri, and George Smoot. "A Brief History of Gravitational Waves". In: *Universe* 2.3 (Sept. 2016), p. 22. DOI: 10.3390/universe2030022.
- [10] A. Charpentier et al. "Multivariate Archimax copulas". In: *Journal of Multivariate Analysis* 126 (Apr. 2014), pp. 118–136. DOI: 10.1016/j.jmva.2013.12.013.

- [11] R. M. Corless et al. “On the LambertW function”. In: *Advances in Computational Mathematics* 5.1 (Dec. 1996), pp. 329–359. DOI: 10.1007/bf02124750.
- [12] Eric Cormier, Christian Genest, and Johanna G. Nešlehová. “Using B-splines for nonparametric inference on bivariate extreme-value copulas”. In: *Extremes* 17.4 (Aug. 2014), pp. 633–659. DOI: 10.1007/s10687-014-0199-4.
- [13] Data Mechanics. *Docker image for Apache Spark*. URL: <https://hub.docker.com/r/datamechanics/spark> (visited on 09/11/2021).
- [14] Docker, Inc. *Docker. Container technology*. URL: <https://www.docker.com/> (visited on 09/11/2021).
- [15] Gabriel Doyon. “On Densities of Extreme Value Copulas”. MA thesis. Universität Zürich, 2013.
- [16] J. J. Egozcue, J. L. Díaz-Barrero, and V. Pawłowsky-Glahn. “Hilbert Space of Probability Density Functions Based on Aitchison Geometry”. In: *Acta Mathematica Sinica, English Series* 22.4 (Jan. 2006), pp. 1175–1182. DOI: 10.1007/s10114-005-0678-2.
- [17] John H. J. Einmahl and Johan Segers. “Maximum empirical likelihood estimation of the spectral measure of an extreme-value distribution”. In: *The Annals of Statistics* 37.5B (Oct. 2009). DOI: 10.1214/08-aos677.
- [18] Ionas Erb and Nihat Ay. “The Information-Geometric Perspective of Compositional Data Analysis”. In: *Advances in Compositional Data Analysis*. Springer International Publishing, 2021, pp. 21–43. DOI: 10.1007/978-3-030-71175-7_2.
- [19] Patrick Eschenburg. “Properties of extreme-value copulas”. MA thesis. 2013.
- [20] Amèlie Fils-Villetard, Armelle Guillou, and Johan Segers. “Projection estimators of Pickands dependence functions”. In: *Canadian Journal of Statistics* 36.3 (Sept. 2008), pp. 369–382. DOI: 10.1002/cjs.5550360303.
- [21] Andrea Fontanari, Pasquale Cirillo, and Cornelis W. Oosterlee. “Lorenz-generated bivariate Archimedean copulas”. In: *Dependence Modeling* 8.1 (Jan. 2020), pp. 186–209. DOI: 10.1515/demo-2020-0011. URL: <https://www.degruyter.com/document/doi/10.1515/demo-2020-0011/html>.
- [22] Daniel Foreman-Mackey et al. “emcee: The MCMC Hammer”. In: *Publications of the Astronomical Society of the Pacific* 125.925 (Mar. 2013), pp. 306–312. DOI: 10.1086/670067.
- [23] Christian Genest, Johanna Nešlehová, and Jean-François Quessy. “Tests of symmetry for bivariate copulas”. In: *Annals of the Institute of Statistical Mathematics* 64.4 (Sept. 2011), pp. 811–834. DOI: 10.1007/s10463-011-0337-6.
- [24] Christian Genest and Johanna G. Nešlehová. “When Gumbel met Galambos”. In: *Copulas and Dependence Models with Applications*. Springer International Publishing, 2017, pp. 83–93. DOI: 10.1007/978-3-319-64221-5_6.

- [25] Pierre Georges et al. “Multivariate Survival Modelling: A Unified Approach with Copulas”. In: *SSRN Electronic Journal* (2001). DOI: 10.2139/ssrn.1032559.
- [26] Noomen Ben Ghorbal, Christian Genest, and Johanna Nešlehová. “On the Ghoudi, Khoudraji, and Rivest test for extreme-value dependence”. In: *Canadian Journal of Statistics* 37.4 (Dec. 2009), pp. 534–552. DOI: 10.1002/cjs.10034.
- [27] Google Cloud Platform. *Spark Operator. Kubernetes operator for managing the lifecycle of Apache Spark applications on Kubernetes*. URL: <https://operatorhub.io/operator/spark-gcp> (visited on 09/11/2021).
- [28] Gordon Gudendorf and Johan Segers. “Extreme-Value Copulas”. In: *Copula Theory and Its Applications*. Springer Berlin Heidelberg, 2010, pp. 127–145. DOI: 10.1007/978-3-642-12465-5_6.
- [29] Simon Guillotte and François Perron. “Polynomial Pickands functions”. In: *Bernoulli* 22.1 (Feb. 2016), pp. 213–241. DOI: 10.3150/14-bej656.
- [30] Sándor Guzmics and Georg Ch. Pflug. “A new extreme value copula and new families of univariate distributions based on Freund’s exponential model”. In: *Dependence Modeling* 8.1 (Jan. 2020), pp. 330–360. DOI: 10.1515/demo-2020-0018.
- [31] José Miguel Hernández-Lobato and Alberto Suárez. “Semiparametric bivariate Archimedean copulas”. In: *Computational Statistics & Data Analysis* 55.6 (June 2011), pp. 2038–2058. DOI: 10.1016/j.csda.2011.01.018.
- [32] Javier Rojo Jiménez, Enrique Villa-Diharce, and Miguel Flores. “Nonparametric Estimation of the Dependence Function in Bivariate Extreme Value Distributions”. In: *Journal of Multivariate Analysis* 76.2 (Feb. 2001), pp. 159–191. DOI: 10.1006/jmva.2000.1931.
- [33] N. Kamnitui et al. “On the size of the class of bivariate extreme-value copulas with a fixed value of Spearman's rho or Kendall's tau”. In: *Journal of Mathematical Analysis and Applications* 472.1 (Apr. 2019), pp. 920–936. DOI: 10.1016/j.jmaa.2018.11.057. URL: <https://www.sciencedirect.com/science/article/pii/S0022247X18310035?via=ihub>.
- [34] A. Khoudraji. “Contributions à l’étude des copules et à la modélisation des valeurs extrêmes bivariées”. PhD thesis. Université Laval, Québec, Canada, 1995.
- [35] Chun Kai Ling, Fei Fang, and J. Zico Kolter. “Deep Archimedean Copulas”. In: *34th Conference on Neural Information Processing Systems (NeurIPS 2020)*. Vancouver, Canada, Dec. 5, 2020. arXiv: 2012.03137 [cs.LG].
- [36] Jian Ma and Zengqi Sun. “Mutual information is copula entropy”. In: *Tsinghua Science and Technology* 16.1 (Feb. 2011), pp. 51–54. DOI: 10.1016/s1007-0214(11)70008-6.
- [37] Jitka Machalová et al. “Compositional splines for representation of density functions”. In: *Computational Statistics* (Oct. 2020). DOI: 10.1007/s00180-020-01042-7.

- [38] Dougal Maclaurin, David Duvenaud, and Ryan P. Adams. “Autograd: Effortless gradients in numpy”. In: *ICML 2015 AutoML Workshop*. Vol. 238. 2015, p. 5.
- [39] G. Marcon et al. “Multivariate nonparametric estimation of the Pickands dependence function using Bernstein polynomials”. In: *Journal of Statistical Planning and Inference* 183 (Apr. 2017), pp. 1–17. DOI: 10.1016/j.jspi.2016.10.004.
- [40] Alexander J. McNeil and Johanna Nešlehová. “From Archimedean to Liouville copulas”. In: *Journal of Multivariate Analysis* 101.8 (Sept. 2010), pp. 1772–1790. DOI: 10.1016/j.jmva.2010.03.015.
- [41] Alexander J. McNeil and Johanna Nešlehová. “Multivariate Archimedean copulas, d-monotone functions and ℓ_1 -norm symmetric distributions”. In: *The Annals of Statistics* 37.5B (Oct. 2009), pp. 3059–3097. DOI: 10.1214/07-aos556.
- [42] Roger B. Nelsen. *An Introduction to Copulas*. Springer New York, Nov. 19, 2010. 288 pp. ISBN: 1441921095. URL: https://www.ebook.de/de/product/13633887/roger_b_nelsen_an_introduction_to_copulas.html.
- [43] James Pickands. “Multivariate extreme value distribution”. In: *Proceedings 43th, Session of International Statistical Institution, 1981* (1981).
- [44] Jean-Francois Quessy and Othmane Kortbi. “Minimum-distance statistics for the selection of an asymmetric copula in Khoudraji's class of models”. In: *Statistica Sinica* (2016). DOI: 10.5705/ss.202014.0082.
- [45] Friedrich Schmid and Rafael Schmidt. “Nonparametric inference on multivariate versions of Blomqvist’s beta and related measures of tail dependence”. In: *Metrika* 66.3 (Dec. 2006), pp. 323–354. DOI: 10.1007/s00184-006-0114-3.
- [46] Volker Schmitz. “Copulas and Stochastic Processes”. PhD thesis. Aachen: Rheinisch-Westfälischen Technischen Hochschule Aachen, Jan. 21, 2003. ISBN: 3-8322-1278-7. URL: <https://d-nb.info/972691669/34>.
- [47] Larry I. Schumaker. “On Shape Preserving Quadratic Spline Interpolation”. In: *SIAM Journal on Numerical Analysis* 20.4 (Aug. 1983), pp. 854–864. DOI: 10.1137/0720057.
- [48] The Apache Software Foundation. *Spark. A unified analytics engine for large-scale data processing*. Version 3.1.1. Mar. 2, 2021. URL: <https://spark.apache.org/> (visited on 09/11/2021).
- [49] The Cloud Native Computing Foundation. *Kubernetes. Production-Grade Container Scheduling and Management*. URL: <https://kubernetes.io/> (visited on 09/11/2021).
- [50] The Python Software Foundation. *Python. Programming language*. Version 3.8. Oct. 14, 2019. URL: <https://www.python.org/> (visited on 09/11/2021).
- [51] Alexandre B. Tsybakov. *Introduction to Nonparametric Estimation*. Springer New York, 2009. DOI: 10.1007/b13794.

- [52] Sabrina Vettori, Raphaël Huser, and Marc G. Genton. “A comparison of dependence function estimators in multivariate extremes”. In: *Statistics and Computing* 28.3 (May 2017), pp. 525–538. DOI: 10.1007/s11222-017-9745-7.
- [53] William C. Waterhouse. “Uniform Convergence and Graph Convergence”. In: *The American Mathematical Monthly* 83.8 (Oct. 1976), p. 641. DOI: 10.2307/2319894.